the anterior lens epithelium but not in the acellular capsule and the cornea (**Supplementary Figs. 7** and **9**). The optic nerve glia and vascular endothelial cells also showed positive immunoreactivity for CACNA1A (**Supplementary Fig. 9**). For the retina, we observed strong, diffuse CACNA1A staining in the photoreceptor inner segments, inner nuclear layer (INL) and outer nuclear layer (ONL), and nerve fiber layer (NFL) of non-XFS globes in comparison to XFS globes, where we observed focal and patchy immunostaining of the inner segments, ONL, INL and NFL. Light-microscopy comparison of the irides in XFS-affected eyes against eyes without XFS identified typical XFS findings of exfoliated material on the posterior iris and atrophic iris pigment epithelium, as well as possible atrophy of the iris dilator muscle, in XFS-affected eyes (**Fig. 3**). We also performed double-immunofluorescence microscopy for CACNA1A and LOXL1 in human eyes with and without XFS and observed colocalization of CACNA1A and LOXL1 only in the epithelium of the ciliary processes. The exfoliated material in eyes with XFS showed LOXL1-positive staining with negligible CACNA1A immunoreactivity. The ciliary body and iris smooth musculature had CACNA1A-positive immunostaining but were negative for LOXL1 staining in eyes with and without XFS (**Fig. 3**). This observation raises the possibility that CACNA1A and LOXL1 contribute to XFS pathology through different mechanisms at different ocular sites.

In summary, we have identified a susceptibility locus for XFS mapping to *CACNA1A* using a three-stage GWAS study design. Further investigation of this locus is now warranted to uncover the mechanisms through which CACNA1A affects individual susceptibility to XFS.

**URLs.** Illumina, http://www.illumina.com/; Sequenom, https://www.sequenom.com/; Applied Biosystems, http://www.appliedbiosystems.com/; PLINK, http://pngu.mgh.harvard.edu/~purcell/plink/; R statistical program package, http://www.r-project.org/; IMPUTE2, http://mathgen.stats.ox.ac.uk/impute/impute_v2.html.

## METHODS

Methods and any associated references are available in the online version of the paper.

*Note: Any Supplementary Information and Source Data files are available in the online version of the paper.*

ACKNOWLEDGMENTS

The authors thank the staff and participants of all studies for their important contributions. We thank K.-K. Heng, X.-Y. Chen, H.-M. Soo, S.-Q. Mok, A. Jamuth, N. Foxworth and M. Elbl for technical assistance. This research was funded by the Biomedical Research Council, Agency for Science, Technology and Research, Singapore. J.L.W. acknowledges support from US National Institutes of Health/National Eye Institute grants (NIH/NEI R01 EY020928 and NIH/NEI P30 EY014104). S.W.M.J. acknowledges support from grant EY11721 from the US National Institutes of Health/National Eye Institute and is an investigator of the Howard Hughes Medical Institute. L.R.P. acknowledges support from a Harvard Medical School Distinguished Ophthalmology Scholar Award and the Harvard Glaucoma Center of Excellence. J.H.F. acknowledges support from US National Institutes of Health/National Eye Institute grants (EY023512 and EY018825). Z.Y. acknowledges support from the National Natural Science Foundation of China (81025006 and 81170883), as well as from the Department of Science and Technology of Sichuan Province, China (2012SZ0219 and 2011jtd0020). M.S. acknowledges support from Robert Bosch Stiftung (Stuttgart, Germany) and the German Cancer Consortium (DKTK), Germany. The Australian case cohort was funded by grants from the Ophthalmic Research Institute of Australia and National Health and Medical Research Council (NHMRC) project 535044. The Thessaloniki Eye Study was cofunded by the European Union (European Social Fund) and Greek national funds under act 'Aristia' of the operational program 'Education and Lifelong Learning' (**Supplementary Note**). Blue Mountains Eye Study (BMES) GWAS and genotyping costs were supported by the Australian NHMRC (Canberra, Australia; NHMRC project grants 512423, 475604 and 529912) and the Wellcome Trust, UK, as part of the Wellcome Trust Case Control Consortium 2 (A. Viswanathan, P. McGuffin, P. Mitchell, F. Topouzis, P. Foster; grants 085475/B/08/Z and 085475/08/Z). K.P.B. is an NHMRC Senior Research Fellow, and J.E.C. is an NHMRC Practitioner Fellow. M.A.B. is an NHMRC Principal Research Fellow. A.W.H. is an NHMRC Peter Doherty Fellow.

AUTHOR CONTRIBUTIONS

T.A., M.O. and C.-C.K. conceived the project. M.O., T.M., R.R.A., A.H., S.N., J.E.C., A.W.H., D.A.M., P.M., J.J.W., Y.S.A., J.C.Z., Y.N., T.Z., M.P., L.J., Y.X.W., S.W., D.P., P.G.S., Y.I., R.S.K., M.U., S. Manabe, K.H., S. Kazama, R.I., Y.M., K. Miyata, K.S., T.H., E.C., K.I., S.I., A.Y., M.Y., Y.K., M.A., T.O., T. Sakurai, T. Sugimoto, H.C., K.Y., S.Y.A., E.A.O., S.A.A.-O., O.O., L.A.-J., S.A.S., Y.Y., Ç.O., M.R.K., A.N.B., S.Y., E.L.A., E.K.-J., U.L., P.C., R.M.R., A.Z., T.C., R. Ramakrishnan, K.N., R.V., P.Z., X.C., D.G.-V., S.A.P., R.H., S.-L.H., U.-C.W.-L., C.M., U.S.-S., S. Moebus, N. Weisschuh, R.S., A.G., I.L., J.G.C., M.C., Q.Y., V.V., P. Founti, A.C., A.L., E.A., A.L.C., M.R.W., D.J.R., I.M.-B., K. Mori, S. Heegaard, W.L.M.A., J.B.J., L.X., J.M.L., F.L., N. Wang, P. Frezzotti, S. Kinoshita, J.H.F., M.I., D.P.E., L.R.P., T.K., J.L.W., F.T., N.Y. and R. Ritch conducted patient recruitment and phenotyping. Z.L., S.U., M.K., K.P.B., M.A.B., J.J.W., Y.G., K.-Y.T., L.H., P.S., W.Y.M., S.Q.P., B.Z., J.S., N.Z., Z.Y. and S.V. performed genotyping experiments. J.M.H., A.S.Y.C., M.C.L., E.N.V., G.R.H. and S.W.M.J. led and performed immunohistochemistry and immunofluorescence experiments. Z.L., K.P.B., R.A.F., P.L., K.K.A.-A., L.A.S., L.H., K.S.S., J.N.F., M.N., F.M., N.G., M.M., S.U., M.K., Y.Y.T., J.H.K., A.E.A.K., S. Herms, Y.L., K.T., B.Z., J.S., N.Z., S.V., Z.Y., G.R.H., P.S., A.C.O., F.P. and A.G. performed analysis. E.N.V., T.Y.W., C.Y.C., P.S., A.M.H., M.M.N., B.C., E.S., M.S. and A.R. contributed genetic and genotyping data from control populations. The manuscript was drafted by C.-C.K., with critical input from T.A., R.R.A., L.R.P., J.L.W., F.P., F.T., M.D., S.W.M.J., R. Ritch and M.A.H. The manuscript was approved by all authors. C.-C.K. was responsible for obtaining financial support for this study.

COMPETING FINANCIAL INTERESTS

The authors declare no competing financial interests.



1. Schlötzer-Schrehardt, U. & Naumann, G.O. Ocular and systemic pseudoexfoliation syndrome. *Am. J. Ophthalmol.* **141**, 921–937 (2006).
2. Ritch, R. & Schlotzer-Schrehardt, U. Exfoliation syndrome. *Surv. Ophthalmol.* **45**, 265–315 (2001).
3. Thorleifsson, G. *et al.* Common sequence variants in the *LOXL1* gene confer susceptibility to exfoliation glaucoma. *Science* **317**, 1397–1400 (2007).
4. Chen, H. *et al.* Ethnicity-based subgroup meta-analysis of the association of *LOXL1* polymorphisms with glaucoma. *Mol. Vis.* **16**, 167–177 (2010).
5. Fingert, J.H. *et al. LOXL1 mutations are associated with exfoliation syndrome in* patients from the midwestern United States. *Am. J. Ophthalmol.* **144**, 974–975 (2007).
6. Hayashi, H., Gotoh, N., Ueda, Y., Nakanishi, H. & Yoshimura, N. Lysyl oxidase–like 1 polymorphisms and exfoliation syndrome in the Japanese population. *Am. J. Ophthalmol.* **145**, 582–585 (2008).
7. Fan, B.J. *et al.* DNA sequence variants in the *LOXL1* gene are associated with pseudoexfoliation glaucoma in a U.S. clinic-based population with broad ethnic diversity. *BMC Med. Genet.* **9**, 5 (2008).
8. Yang, X. *et al.* Genetic association of *LOXL1* gene variants and exfoliation glaucoma in a Utah cohort. *Cell Cycle* **7**, 521–524 (2008).
9. Hewitt, A.W. *et al.* Ancestral *LOXL1* variants are associated with pseudoexfoliation in Caucasian Australians but with markedly lower penetrance than in Nordic people. *Hum. Mol. Genet.* **17**, 710–716 (2008).
10. Pasutto, F. *et al.* Association of *LOXL1* common sequence variants in German and Italian patients with pseudoexfoliation syndrome and pseudoexfoliation glaucoma. *Invest. Ophthalmol. Vis. Sci.* **49**, 1459–1463 (2008).
11. Ozaki, M. *et al.* Association of *LOXL1* gene polymorphisms with pseudoexfoliation in the Japanese. *Invest. Ophthalmol. Vis. Sci.* **49**, 3976–3980 (2008).
12. Fan, B.J. *et al. LOXL1* promoter haplotypes are associated with exfoliation syndrome in a U.S. Caucasian population. *Invest. Ophthalmol. Vis. Sci.* **52**, 2372–2378 (2011).
13. Wolf, C. *et al.* Lysyl oxidase–like 1 gene polymorphisms in German patients with normal tension glaucoma, pigmentary glaucoma and exfoliation glaucoma. *J. Glaucoma* **19**, 136–141 (2010).
14. Lemmelä, S. *et al.* Association of *LOXL1* gene with Finnish exfoliation syndrome patients. *J. Hum. Genet.* **54**, 289–297 (2009).
15. Aragon-Martin, J.A. *et al.* Evaluation of *LOXL1* gene polymorphisms in exfoliation syndrome and exfoliation glaucoma. *Mol. Vis.* **14**, 533–541 (2008).
16. Chen, L. *et al.* Evaluation of *LOXL1* polymorphisms in exfoliation syndrome in a Chinese population. *Mol. Vis.* **15**, 2349–2357 (2009).
17. Mossböck, G. *et al.* Lysyl oxidase–like protein 1 (*LOXL1*) gene polymorphisms and exfoliation glaucoma in a Central European population. *Mol. Vis.* **14**, 857–861 (2008).

18. Challa, P. *et al.* Analysis of *LOXL1* polymorphisms in a United States population with pseudoexfoliation glaucoma. *Mol. Vis.* **14**, 146–149 (2008).
19. Ramprasad, V.L. *et al.* Association of non-synonymous single nucleotide polymorphisms in the *LOXL1* gene with pseudoexfoliation syndrome in India. *Mol. Vis.* **14**, 318–322 (2008).
20. Nakano, M. *et al.* Novel common variants and susceptible haplotype for exfoliation glaucoma specific to Asian population. *Sci. Rep.* **4**, 5340 (2014).
21. Mori, K. *et al. LOXL1* genetic polymorphisms are associated with exfoliation glaucoma in the Japanese population. *Mol. Vis.* **14**, 1037–1040 (2008).
22. Williams, S.E. *et al.* Major *LOXL1* risk allele is reversed in exfoliation glaucoma in a black South African population. *Mol. Vis.* **16**, 705–712 (2010).
23. Krumbiegel, M. *et al.* Genome-wide association study with DNA pooling identifies variants at *CNTNAP2* associated with pseudoexfoliation syndrome. *Eur. J. Hum. Genet.* **19**, 186–193 (2011).
24. Rioux, J.D. *et al.* Genetic variation in the 5q31 cytokine gene cluster confers susceptibility to Crohn disease. *Nat. Genet.* **29**, 223–228 (2001).
25. Westra, H.J. *et al.* Systematic identification of *trans* eQTLs as putative drivers of known disease associations. *Nat. Genet.* **45**, 1238–1243 (2013).
26. Boyle, A.P. *et al.* Annotation of functional variation in personal genomes using RegulomeDB. *Genome Res.* **22**, 1790–1797 (2012).
27. Ward, L.D. & Kellis, M. HaploReg: a resource for exploring chromatin states, conservation, and regulatory motif alterations within sets of genetically linked variants. *Nucleic Acids Res.* **40**, D930–D934 (2012).
28. Schlötzer-Schrehardt, U., Kortje, K.H. & Erb, C. Energy-filtering transmission electron microscopy (EFTEM) in the elemental analysis of pseudoexfoliative material. *Curr. Eye Res.* **22**, 154–162 (2001).
29. Reinhardt, D.P., Ono, R.N. & Sakai, L.Y. Calcium stabilizes fibrillin-1 against proteolytic degradation. *J. Biol. Chem.* **272**, 1231–1236 (1997).

Tin Aung[1–5,99], Mineo Ozaki[6,7,99], Takanori Mizoguchi[8,99], R Rand Allingham[9,99], Zheng Li[4], Aravind Haripriya[10], Satoko Nakano[11], Steffen Uebe[12], Jeffrey M Harder[13], Anita S Y Chan[1,2], Mei Chin Lee[1], Kathryn P Burdon[14,15], Yury S Astakhov[16], Khaled K Abu-Amero[17,18], Juan C Zenteno[19,20], Yildirim Nilgün[21], Tomasz Zarnowski[22], Mohammad Pakravan[23], Leen Abu Safieh[24], Liyun Jia[25], Ya Xing Wang[26], Susan Williams[27], Daniela Paoli[28], Patricio G Schlottmann[29], Lulin Huang[30–32], Kar Seng Sim[4], Jia Nee Foo[4], Masakazu Nakano[33], Yoko Ikeda[34], Rajesh S Kumar[35], Morio Ueno[34], Shin-ichi Manabe[7], Ken Hayashi[7], Shigeyasu Kazama[36], Ryuichi Ideta[37], Yosai Mori[38], Kazunori Miyata[38,39], Kazuhisa Sugiyama[40], Tomomi Higashide[40], Etsuo Chihara[41], Kenji Inoue[42], Satoshi Ishiko[43], Akitoshi Yoshida[44], Masahide Yanagi[45], Yoshiaki Kiuchi[45], Makoto Aihara[46], Tsutomu Ohashi[47], Toshiya Sakurai[48], Takako Sugimoto[39], Hideki Chuman[39], Fumihiko Matsuda[49], Kenji Yamashiro[50], Norimoto Gotoh[50], Masahiro Miyake[49,50], Sergei Y Astakhov[16], Essam A Osman[17], Saleh A Al-Obeidan[17], Ohoud Owaidhah[23], Leyla Al-Jasim[23], Sami Al Shahwan[23], Rhys A Fogarty[14], Paul Leo[51], Yaz Yetkin[21], Çilingir Oğuz[21], Mozhgan Rezaei Kanavi[23], Afsaneh Nederi Beni[23], Shahin Yazdani[23], Evgeny L Akopov[16], Kai-Yee Toh[4], Gareth R Howell[13], Andrew C Orr[52], Yufen Goh[4], Wee Yang Meah[4], Su Qin Peh[4], Ewa Kosior-Jarecka[22], Urszula Lukasik[22], Mandy Krumbiegel[12], Eranga N Vithana[1], Tien Yin Wong[1–3], Yutao Liu[53,54], Allison E Ashley Koch[53], Pratap Challa[9], Robyn M Rautenbach[55], David A Mackey[56], Alex W Hewitt[15,57], Paul Mitchell[58], Jie Jin Wang[58], Ari Ziskind[55], Trevor Carmichael[27], Rangappa Ramakrishnan[10], Kalpana Narendran[10], Rangaraj Venkatesh[10], Saravanan Vijayan[59], Peiquan Zhao[60], Xueyi Chen[61], Dalia Guadarrama-Vallejo[19,20], Ching Yu Cheng[1,3], Shamira A Perera[1,2], Rahat Husain[1,2], Su-Ling Ho[62], Ulrich-Christoph Welge-Luessen[63], Christian Mardin[63], Ursula Schloetzer-Schrehardt[63], Axel M Hillmer[64], Stefan Herms[65–68], Susanne Moebus[69], Markus M Nöthen[65,66], Nicole Weisschuh[70], Rohit Shetty[35], Arkasubhra Ghosh[1,71], Yik Ying Teo[9,72], Matthew A Brown[51], Ignacio Lischinsky[73], Blue Mountains Eye Study GWAS Team[74], Wellcome Trust Case Control Consortium 2[74], Jonathan G Crowston[57,75], Michael Coote[57,75], Bowen Zhao[24], Jinghong Sang[25], Nihong Zhang[25], Qisheng You[26], Vera Vysochinskaya[76], Panayiota Founti[77], Anthoula Chatzikyriakidou[78], Alexandros Lambropoulos[78], Eleftherios Anastasopoulos[77], Anne L Coleman[79], M Roy Wilson[80], Douglas J Rhee[81], Jae Hee Kang[82], Inna May-Bolchakova[83], Steffen Heegaard[84,85], Kazuhiko Mori[33], Wallace L M Alward[86,87], Jost B Jonas[88], Liang Xu[26], Jeffrey M Liebmann[89], Balram Chowbay[90], Elke Schaeffeler[91], Matthias Schwab[91–93], Fabian Lerner[94], Ningli Wang[25], Zhenglin Yang[30–32], Paolo Frezzotti[95], Shigeru Kinoshita[34], John H Fingert[86,87], Masaru Inatani[96], Kei Tashiro[33], André Reis[12], Deepak P Edward[24,97], Louis R Pasquale[81,82], Toshiaki Kubota[11], Janey L Wiggs[81,100], Francesca Pasutto[12,100], Fotis Topouzis[77,100], Michael Dubina[16,76,100], Jamie E Craig[14,100], Nagahisa Yoshimura[50,100], Periasamy Sundaresan[59,100], Simon W M John[13,100], Robert Ritch[98,100], Michael A Hauser[9,53,100] & Chiea-Chuen Khor[1,3,4,100]

[1]Singapore Eye Research Institute, Singapore. [2]Singapore National Eye Center, Singapore. [3]Department of Ophthalmology, Yong Loo Lin School of Medicine, National University of Singapore, Singapore. [4]Division of Human Genetics, Genome Institute of Singapore, Singapore. [5]Duke University–National University of Singapore Graduate Medical School, Singapore. [6]Ozaki Eye Hospital, Hyuga, Japan. [7]Hayashi Eye Hospital, Fukuoka, Japan. [8]Mizoguchi Eye Hospital, Sasebo, Japan. [9]Department of Ophthalmology, Duke University Eye Center, Durham, North Carolina, USA. [10]Intraocular Lens and Cataract Clinic, Aravind Eye Hospital, Madurai, India. [11]Department of Ophthalmology, Oita University Faculty of Medicine, Oita, Japan. [12]Institute of Human Genetics, Friedrich Alexander Universität Erlangen-Nürnberg, Erlangen-Nürnberg, Germany. [13]Howard Hughes Medical Institute, Jackson Laboratory, Bar Harbor, Maine, USA. [14]Department of Ophthalmology, Flinders University, Adelaide, South Australia, Australia. [15]Menzies Institute for Medical Research, University of Tasmania, Hobart, Tasmania, Australia. [16]Department of Ophthalmology, First Pavlov State Medical University of St. Petersburg, St. Petersburg, Russia. [17]Department of Ophthalmology, College of Medicine, King Saud

University, Riyadh, Saudi Arabia. [18]Department of Ophthalmology, College of Medicine, University of Florida, Jacksonville, Florida, USA. [19]Department of Genetics, Institute of Ophthalmology Conde de Valenciana, Mexico City, Mexico. [20]Department of Biochemistry, Faculty of Medicine, Universidad Nacional Autónoma de México, Mexico City, Mexico. [21]Department of Ophthalmology, Eskisehir Osmangazi University, Meselik, Turkey. [22]Department of Diagnostics and Microsurgery of Glaucoma, Medical University, Lublin, Poland. [23]Department of Ophthalmology, Ophthalmic Research Center, Labbafinejad Medical Center, Shahid Beheshti University of Medical Sciences, Tehran, Iran. [24]King Khaled Eye Specialist Hospital, Riyadh, Saudi Arabia. [25]Beijing Ophthalmology and Visual Sciences Key Laboratory, Beijing Tongren Eye Centre, Beijing Tongren Hospital, Capital Medical University, Beijing, China. [26]Beijing Institute of Ophthalmology, Beijing Tongren Hospital, Capital University of Medical Science, Beijing, China. [27]Division of Ophthalmology, Department of Neurosciences, University of the Witwatersrand, Johannesburg, South Africa. [28]Department of Ophthalmology, Monfalcone Hospital, Gorizia, Italy. [29]Organización Médica de Investigación, Buenos Aires, Argentina. [30]Sichuan Provincial Key Laboratory for Human Disease Gene Study, Hospital of the University of Electronic Science and Technology of China and Sichuan Provincial People's Hospital, Chengdu, China. [31]School of Medicine, University of Electronic Science and Technology of China, Chengdu, China. [32]Sichuan Translational Medicine Hospital, Chinese Academy of Sciences, Chengdu, China. [33]Department of Genomic Medical Sciences, Kyoto Prefectural University of Medicine, Kyoto, Japan. [34]Department of Ophthalmology, Kyoto Prefectural University of Medicine, Kyoto, Japan. [35]Glaucoma Services, Narayana Nethralaya Eye Hospital, Bangalore, India. [36]Shinjo Eye Clinic, Miyazaki, Japan. [37]Ideta Eye Hospital, Kumamoto, Japan. [38]Miyata Eye Hospital, Miyazaki, Japan. [39]Department of Ophthalmology, Faculty of Medicine, University of Miyazaki, Miyazaki, Japan. [40]Department of Ophthalmology and Visual Science, Kanazawa University Graduate School of Medical Science, Kanazawa University, Kanazawa, Japan. [41]Sensho-kai Eye Institute, Kyoto, Japan. [42]Inouye Eye Hospital, Tokyo, Japan. [43]Department of Medicine and Engineering Combined Research Institute, Asahikawa Medical University, Asahikawa, Japan. [44]Department of Ophthalmology, Asahikawa Medical University, Asahikawa, Japan. [45]Department of Ophthalmology and Visual Science, Hiroshima University, Hiroshima, Japan. [46]Yotsuya Shirato Eye Clinic, Tokyo, Japan. [47]Ohashi Eye Center, Sapporo, Japan. [48]Tane Memorial Eye Hospital, Osaka, Japan. [49]Center for Genomic Medicine/INSERM U852, Kyoto University Graduate School of Medicine, Kyoto, Japan. [50]Department of Ophthalmology and Visual Sciences, Kyoto University Graduate School of Medicine, Kyoto, Japan. [51]University of Queensland Diamantina Institute, Translational Research Institute, Princess Alexandra Hospital, Brisbane, Queensland, Australia. [52]Department of Ophthalmology and Visual Sciences, Dalhousie University, Halifax, Nova Scotia, Canada. [53]Department of Medicine, Duke University Medical Center, Durham, North Carolina, USA. [54]Department of Cellular Biology and Anatomy, Georgia Regents University, Augusta, Georgia, USA. [55]Division of Ophthalmology, Faculty of Medicine and Health Sciences, University of Stellenbosch, Cape Town, South Africa. [56]Centre for Ophthalmology and Visual Science, Lions Eye Institute, University of Western Australia, Perth, Western Australia, Australia. [57]Centre for Eye Research Australia (CERA), University of Melbourne, Royal Victorian Eye and Ear Hospital, Melbourne, Victoria, Australia. [58]Centre for Vision Research, Department of Ophthalmology and Westmead Millennium Institute, University of Sydney, Sydney, New South Wales, Australia. [59]Department of Genetics, Aravind Medical Research Foundation, Madurai, India. [60]Department of Ophthalmology, Xin Hua Hospital affiliated to Shanghai Jiao Tong University, School of Medicine, Shanghai, China. [61]Department of Ophthalmology, First Affiliated Hospital of Xinjiang Medical University, Urumchi, Xinjiang Uygur Autonomous Region, China. [62]National Healthcare Group Eye Institute, Tan Tock Seng Hospital, Singapore. [63]Department of Ophthalmology, Friedrich Alexander Universität Erlangen-Nürnberg, Erlangen-Nürnberg, Germany. [64]Cancer Therapeutics and Stratified Oncology, Genome Institute of Singapore, Singapore. [65]Institute of Human Genetics, University of Bonn, Bonn, Germany. [66]Department of Genomics, Life & Brain Center, University of Bonn, Bonn, Germany. [67]Division of Medical Genetics, University Hospital, Basel, Switzerland. [68]Human Genetics Research Group, Department of Biomedicine, University of Basel, Basel, Switzerland. [69]Institute for Medical Informatics, Biometry and Epidemiology, University Hospital of Essen, University Duisburg-Essen, Essen, Germany. [70]University Eye Hospital, Würzburg, Germany. [71]Genes, Repair and Regeneration in Ophthalmic Workstation Research Laboratory, Narayana Nethralaya Foundation, Bangalore, India. [72]Saw Swee Hock School of Public Health, National University of Singapore, Singapore. [73]Centro Oftalmológico Lischinsky, Tucumán, Argentina. [74]A full list of members and affiliations appears in the **Supplementary Note**. [75]Department of Ophthalmology, University of Melbourne, Melbourne, Victoria, Australia. [76]St. Petersburg Academic University, St. Petersburg, Russia. [77]Department of Ophthalmology, Faculty of Medicine, Aristotle University of Thessaloniki, American Hellenic Educational Progressive Association Hospital, Thessaloniki, Greece. [78]Department of Biology and Genetics, Faculty of Medicine, Aristotle University of Thessaloniki, Thessaloniki, Greece. [79]Center for Community Outreach and Policy, Stein Eye Institute, David Geffen School of Medicine at the University of California, Los Angeles, Los Angeles, California, USA. [80]Wayne State University, Detroit, Michigan, USA. [81]Department of Ophthalmology, Harvard Medical School, Massachusetts Eye and Ear Infirmary, Boston, Massachusetts, USA. [82]Channing Division of Network Medicine, Brigham and Women's Hospital, Boston, Massachusetts, USA. [83]Department of Ophthalmology, Military Hospital Begin, Paris, France. [84]Eye Pathology Institute, Department of Neuroscience and Pharmacology, University of Copenhagen, Copenhagen, Denmark. [85]Department of Ophthalmology, Glostrup University Hospital, Glostrup, Denmark. [86]Stephen A. Wynn Institute for Vision Research, University of Iowa, Iowa City, Iowa, USA. [87]Department of Ophthalmology and Visual Sciences, Carver College of Medicine, University of Iowa, Iowa City, Iowa, USA. [88]Department of Ophthalmology, Medical Faculty Mannheim of the Ruprecht Karls University Heidelberg, Heidelberg, Germany. [89]New York University School of Medicine, Manhattan Eye, Ear and Throat Hospital, New York, New York, USA. [90]Division of Medical Sciences, Humphrey Oei Institute of Cancer Research, National Cancer Centre of Singapore, Singapore. [91]Dr. Margarete Fischer-Bosch Institute of Clinical Pharmacology, Stuttgart, Germany. [92]Department of Clinical Pharmacology, University Hospital, Tübingen, Germany. [93]German Cancer Consortium (DKTK), German Cancer Research Center, Heidelberg, Germany. [94]Fundación para el Estudio del Glaucoma, Buenos Aires, Argentina. [95]Department of Surgery, Section of Ophthalmology, University of Siena, Siena, Italy. [96]Department of Ophthalmology, Faculty of Medical Science, University of Fukui, Fukui, Japan. [97]Wilmer Eye Institute, Johns Hopkins University School of Medicine, Baltimore, Maryland, USA. [98]Einhorn Clinical Research Center, New York Eye and Ear Infirmary of Mount Sinai, New York, New York, USA. [99]These authors contributed equally to this work. [100]These authors jointly supervised this work. Correspondence should be addressed to T.A. (aung_tin@yahoo.co.uk) or C.-C.K. (khorcc@gis.a-star.edu.sg).

## ONLINE METHODS

**Patient recruitment.** Detailed information on all XFS sample collections can be found in the **Supplementary Note**. All cases and controls were enrolled in the study following informed consent and ethical approval from the relevant national and regional institutional review boards for each sample collection. DNA was extracted from patient blood samples using standard, well-described laboratory procedures for genetic analysis.

**Genotyping.** For the GWAS discovery stage, genome-wide genotyping was performed using Illumina OmniExpress BeadChips, following the manufacturer's instructions (see URLs). For validation (stage 1), genotyping was performed using the Sequenom MassARRAY platform (see URLs). For replication (stage 2), genotyping was performed using Applied Biosystems TaqMan probes (see URLs) for samples from India, Germany, Italy, China, Iran, Poland and Argentina. The Australian replication collection had GWAS genotyping for all cases and controls using Illumina genome-wide arrays, and *CACNA1A* rs4926244 was directly genotyped on the GWAS arrays. We performed cross-platform concordance checks and verified >99.9% concordance of genotypes for the SNP markers of interest reported here (for example, rs4926244).

**Statistical analysis.** Stringent quality control filters were used to remove poorly performing samples and SNP markers in both the GWAS discovery and validation phases. SNPs with call rate <95%, with minor allele frequency <1% or showing significant deviation from Hardy-Weinberg equilibrium ($P$ value for deviation $< 1 \times 10^{-6}$) were removed from further statistical analysis. Likewise, samples with an overall genotyping success rate of less than 95% were removed from further analysis. The remaining samples were then subjected to biological relationship verification using the principle of variability in allele sharing. Identity-by-state information was derived using PLINK (see URLs). For those pairs of individuals who showed evidence of cryptic relatedness (possibly either due to duplicated or biologically related samples), we removed the sample with the lower call rate before performing principal-component analysis (PCA). PCA was undertaken to account for spurious associations resulting from ancestral differences for individual SNPs, and principal-component plots were generated using the R statistical program package (see URLs). For the GWAS discovery stage, all XFS cases had genetically matched controls, as visualized spatially by PCA (**Supplementary Fig. 11**). A total of 581,023 autosomal SNPs passed quality filters for call rate and minor allele frequency and were included for further analysis. Genotypes were contrasted between XFS cases and controls using logistic regression, with adjustments for the top six principal components of genetic ancestry to further minimize confounding due to cryptic population stratification. We did not observe any evidence of genomic inflation ($\lambda_{GC} = 1$; **Supplementary Fig. 12**), suggesting that the association results were not confounded by external artifacts such as genetic mismatch between cases and controls. Crucially, we did not observe any deviation or dispersion of test statistics when patients with XFS without glaucoma were compared to patients with exfoliation glaucoma (**Supplementary Fig. 13**). This suggests that our primary analysis approach in combining all patients with XFS into an overall case group is valid.

For the GWAS discovery, validation and replication stages, analysis of association with XFS disease status was carried out using allele-based score tests (1 degree of freedom), which modeled additive effects of the minor allele on disease risk. For the GWAS discovery stage, we incorporated the top six principal components of genetic stratification into the logistic regression model while performing the analysis for association to minimize the effect of residual population stratification. As the follow-up validation (stage 1) and replication (stage 2) phases only tested a limited number of genetic markers, we were unable to adjust for population stratification in these follow-up sample collections. However, association tests were performed by site to minimize population stratification, and statistics were subsequently combined in meta-analysis as described below. All $P$ values reported here are two-tailed.

Meta-analysis was conducted using inverse variance weights for each sample collection, calculating an overall $z$ statistic, its corresponding $P$ value and an accompanying OR estimate for each SNP analyzed. The meta-analysis was performed under the fixed-effects model[30]. Analysis of LD was performed using the R software package (version 2.9.0) and associated rmeta and RColorBrewer analytical packages.

**Genotype imputation.** Fine-scale imputation at *CACNA1A* was performed using all 1,484 XFS cases and 1,188 controls passing the standard GWAS quality control checks. Imputation and phasing of genotypes were carried out using IMPUTE2 (see URLs) with cosmopolitan population haplotypes based on data from 2,535 individuals from 26 distinct populations around the world obtained from the 1000 Genomes Project Phase 3 release (June 2014) for reference panel construction. Imputed genotypes were called with an impute probability threshold of 0.90, with all other genotypes classified as missing. Additional quality control filters were applied to remove SNPs with a call rate <99% should the SNP have a minor allele frequency below 5% in either cases or controls. For common SNPs with a minor allele frequency >5%, the filtering criterion was set at a call rate of <95%.

**Power calculations.** All statistical power calculations were performed as previously described[31]. We present these power calculations for each of the following conditions: (i) the GWAS discovery stage only; (ii) the GWAS discovery stage plus stage 1 validation; and (iii) the GWAS discovery stage plus stage 1 validation plus stage 2 replication (**Supplementary Table 9**).

**Expression analysis.** Multiple transcript variants encoding different isoforms have been found for *CACNA1A*. Here we assessed the presence of either of the two major transcripts known for *CACNA1A*, which encode 2,506- and 2,261-residue proteins, $Ca_V2.1$ variants 1 and 2, respectively ($Ca_V2.1$_V2 and $Ca_V2.1$_V1; NCBI, NM_001127222.1, NP_001120694.1 and NM_001127221.1, NP_001120693.1). All of the known critical regulatory elements of the $Ca_V2.1$ C-terminal tail are included in both variants, but the polyQ domain is excluded from the short-tailed $Ca_V2.1$_V1 isoform[32]. We used five pairs of primers spread across and common to both transcripts to assess the presence of each transcript in eye tissues (**Supplementary Table 10**). *CACNA1A* transcript expression was assessed by semiquantitative RT-PCR using the above-mentioned *CACNA1A*-specific primers on total RNA extracted from a variety of ocular tissues (anterior sclera, cornea, iris, trabecular meshwork, lens capsule, retina, choroid, optic nerve head and optic nerve) with TRIzol reagent (Invitrogen) in accordance with the manufacturer's protocol. First-strand cDNA synthesis was performed with the SuperScript First-Strand Synthesis System for RT-PCR (Invitrogen). Semiquantitative RT-PCR was performed according to the manufacturer's protocol with SYBR Green Master Mix (Invitrogen) using the above *CACNA1A* primers. RT-PCR products were separated on a 2% agarose gel and visualized by ethidium bromide staining. The ubiquitously expressed *ACTB* gene (encoding β-actin) was amplified using specific primers (**Supplementary Table 10**) and used as an amplification and normalizing control.

**Protein blotting.** Cell lines obtained from the American Type Culture Collection included a human retinal pigment epithelial cell line (APRE-19), a human cervical adenocarcinoma cell line (HeLa S), a human breast adenocarcinoma cell line (MCF-7) and a human embryonic kidney epithelial cell line (HEK293). A human nonpigmented ciliary epithelial cell line (NPCE) was a kind gift from M. Coca-Prados (Yale School of Medicine). A human trabecular meshwork cell line (HTM) was purchased from PromoCell and tested for mycoplasma. Cell lysates were obtained by lysing individual cell lines with lysis buffer (50 mM Tris-HCl, pH 8, 150 mM NaCl, 1.0% Nonidet P-40, 0.5% deoxycholate, 0.1% SDS, 0.2 mM $NaVO_4$, 10 mM sodium fluoride, 0.4 mM EDTA and 10% glycerol). Proteins resolved by SDS-PAGE were transferred to HyBond-C Extra nitrocellulose membranes (Amersham Life Science). Membranes were blocked with 5% nonfat milk, 0.1% Tween-20 in Tris-buffered saline (20 mM Tris-HCl, pH 7.6, 150 mM NaCl) for 1 h before incubation with antibody to CACNA1A (1:1,000 dilution; ab81011, Abcam) and antibody to actin conjugated to horseradish peroxidase (HRP) (1:50,000 dilution; sc-47778, Santa Cruz Biotechnology). Blocking and blotting with antibodies were performed in 10% horse serum (Sigma-Aldrich), 0.1% Tween-20 in PBS for 1 h. Bound primary antibodies were detected by HRP-conjugated secondary antibodies (GE Healthcare Biosciences), and signals were visualized with Luminata Forte Western HRP substrate (Millipore).

**Immunofluorescence confocal microscopy.** Immunofluorescence confocal microscopy was performed on 4-μm paraffin sections after antigen retrieval. Blocking of tissue sections was performed with blocking buffer (10% FBS, 0.1% PBS-Tween-20; 1× penicillin and streptomycin) for 1 h at room temperature. Antibodies to CACNA1A (Abcam, ab81011) and LOXL1 (Abnova, H00004016-B01P) were diluted at 1:300 with blocking buffer and incubated with samples overnight at 4 °C. Secondary anti-mouse or anti-rabbit antibodies labeled with FITC (1:300 dilution) or Cy3 (1:300 dilution) (Jackson Labs) were also diluted in blocking buffer and were incubated with samples at room temperature for 1 h followed by application of Vectashield with 4′,6-diamidino-2-phenylindole (DAPI; Vector Laboratories). Coverslips were then used to overlay the sections, and slides were stored in the dark at 4 °C until viewing with an Olympus Fluoview 1000 confocal microscope (Olympus Optical).

**Immunohistochemistry.** A total of seven archival enucleated globes were retrieved for immunohistochemistry analysis with antibodies to CACNA1A (1:50 dilution; Abcam) and LOXL1 (1:50 dilution; Abnova). Three human eye globes from Saudi Arabia and one from Denmark with a history of advanced XFS were obtained courtesy of D.P.E. and S. Heegaard, respectively. Three additional eyes from Singapore (Singapore General Hospital–Singapore National Eye Center Ophthalmic Pathology Service, Singapore General Hospital Pathology) that were exenterated for other external pathological diagnoses that did not involve the globe were used as non-XFS controls. Immunohistochemistry analysis was performed according to our previously published protocol[33]. In brief, paraffin sections were cut at 4 μm and placed on coated slides. Immunohistochemistry was performed using Leica Bond Polymer Refine detection kit DS9800 (Leica Microsystems). Slides were heated for 20 min at 60 °C and then loaded onto the Leica Bond III autostainer for immunohistochemical staining. Staining on the autostainer consisted of dewaxing, antigen retrieval using Leica Bond ER2 solution for 20 min at 100 °C, incubation with antibody for 20 min at room temperature and staining using the Bond polymer refine kit. Polymeric alkaline phosphatase (AP) linker antibody conjugate system (Vision Biosystems) and counterstaining with hematoxylin were applied for visualization, after which slides were dehydrated and coverslips applied.

**Immunofluorescence confocal microscopy in mice.** C57BL/6J and B6(Cg)-Tyrc-2J/J mice were obtained from the Jackson Laboratory production facility. Mice were housed with a 14-h light/10-h dark cycle, under the same conditions as previously described[34]. All experiments were performed in compliance with the Association for Research in Vision and Ophthalmology statement for use of animals in ophthalmic and vision research and approved by the Jackson Laboratory Animal Care and Use Committee. Adult mice were deeply anesthetized and perfused with 1× PBS, and eyes were enucleated. Fresh tissue was frozen in optimal cutting temperature (OCT) compound frozen by liquid nitrogen–cooled isopentane and stored at −80 °C or eyes were fixed overnight in 4% paraformaldehyde. Fixed eyes were cryoprotected in 30% sucrose, rinsed in 1× PBS and frozen in OCT for sectioning. Eyes were cut into 12-μm sections. Primary antibodies used to stain sections included antibodies to CACNA1A (1:500 dilution; AB5152, Millipore), endomucin (EMCN; 1:500 dilution; 14-5851, eBioscience) and smooth muscle actin (ACTA2; 1:500 dilution; ab7817, Abcam). Alexa Fluor–conjugated secondary antibodies from Invitrogen (A-11029 and A-11037) were used to label primary antibodies for immunofluorescence. Sections were desiccated, washed in 1× PBS with 0.5% Triton X-100 and incubated with primary antibodies overnight. Sections were subsequently washed in 1× PBS and incubated with secondary antibodies for 60 min. DAPI was used to stain nuclei. For each experiment, at least four sections from four eyes were assessed. Microscopy was performed on the Axio Imager (Zeiss).


30. Willer, C.J., Li, Y. & Abecasis, G.R. METAL: fast and efficient meta-analysis of genomewide association scans. *Bioinformatics* **26**, 2190–2191 (2010).
31. Purcell, S., Cherny, S.S. & Sham, P.C. Genetic Power Calculator: design of linkage and association genetic mapping studies of complex traits. *Bioinformatics* **19**, 149–150 (2003).
32. Tsou, W.L., Soong, B.W., Paulson, H.L. & Rodriguez-Lebron, E. Splice isoform–specific suppression of the $Ca_V2.1$ variant underlying spinocerebellar ataxia type 6. *Neurobiol. Dis.* **43**, 533–542 (2011).
33. Lee, M.C. *et al.* Expression of the primary angle closure glaucoma (PACG) susceptibility gene *PLEKHA7* in endothelial and epithelial cell junctions in the eye. *Invest. Ophthalmol. Vis. Sci.* **55**, 3833–3841 (2014).
34. Smith, R.S. *et al.* Haploinsufficiency of the transcription factors FOXC1 and FOXC2 results in aberrant ocular development. *Hum. Mol. Genet.* **9**, 1021–1032 (2000).

SCIENTIFIC REPORTS

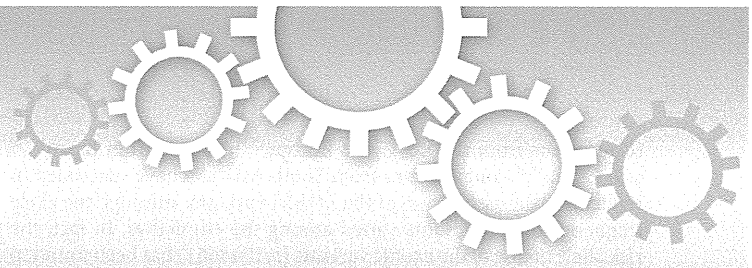

OPEN

SUBJECT AREAS:
GENOME-WIDE ASSOCIATION STUDIES
GENETIC TESTING

Received
13 November 2013

Accepted
28 May 2014

Published
18 June 2014

Correspondence and requests for materials should be addressed to S.K. (shigeruk@koto.kpu-m.ac.jp) or K.T. (tashiro@koto.kpu-m.ac.jp)

* These authors contributed equally to this work.

# Novel common variants and susceptible haplotype for exfoliation glaucoma specific to Asian population

Masakazu Nakano[1]*, Yoko Ikeda[2]*, Yuichi Tokuda[1]*, Masahiro Fuwa[1,3], Morio Ueno[2], Kojiro Imai[2], Ryuichi Sato[1], Natsue Omi[1], Hiroko Adachi[1], Masaaki Kageyama[3], Kazuhiko Mori[2], Shigeru Kinoshita[2] & Kei Tashiro[1]

[1]Department of Genomic Medical Sciences, Kyoto Prefectural University of Medicine, Kyoto, Japan, [2]Department of Ophthalmology, Kyoto Prefectural University of Medicine, Kyoto, Japan, [3]Research and Development Center, Santen Pharmaceutical Co. Ltd., Nara, Japan.

**The common variants in lysyl oxidase-like 1 gene (*LOXL1*) are associated with exfoliation glaucoma (XFG) patients developed through exfoliation syndrome (XFS). However, the risk allele of a variant in *LOXL1* has been found to be inverted between Asian and Caucasian populations. Therefore, we newly performed a genome-wide association study using 201 XFS/XFG and 697 controls in Japanese, and identified 34 genome-wide significant single-nucleotide polymorphisms (SNPs) distributing in not only *LOXL1* but also *TBC1D21* and *PML* at the 15q24.1 locus. These SNPs were confirmed by an independent population consisted of 121 XFS/XFG and 263 controls in Japanese. Moreover, further analyses revealed a unique haplotype structure only from the combination of *TBC1D21* and *LOXL1* variants showing a high XFS/XFG susceptibility specific for the Asian population. Although there still should be other gene(s) in the other region(s) contributing to the disease process, these results suggested that the combination of newly discovered variants in these genes might be useful for precise XFG risk assessment, as well as for elucidating the molecular mechanism of XFG pathogenesis through XFS.**

Glaucoma is one of the leading causes of irreversible blindness worldwide[1]. It is a complex age-related disorder consisting of heterogeneous subtypes that share common features for the development of the disease, i.e., progressive loss of retinal ganglion cells and optic nerve axons that result in visual field defects[2]. Therefore, it is important to investigate each distinct type of glaucoma in order to elucidate the different molecular pathways that lead to the common optic-nerve degeneration.

Exfoliation glaucoma (XFG) is categorized as secondary open-angle glaucoma and reportedly develops from exfoliation syndrome (XFS), as manifested by an observation of abnormal fibrillar deposits (known as pseudoexfoliation (PEX)) on the lens and iris epithelium[3]. In general, XFG has a worse prognosis than primary open-angle glaucoma (POAG), the major type of glaucoma, as it is often observed in patients as elevated intraocular pressure (IOP) combined with severe damage of visual function at the time of initial presentation due to the asymptomatic nature of glaucoma. Moreover, according to the findings reported in the Tajima Study[4], a robust epidemiology study conducted in Japan, XFG accounts for 0.8% of the 5.0% of all types of glaucoma observed in Japanese people over 40 years of age, and the prevalence of XFG increases with advancing age. Consequently, it would be of enormous benefit if the predisposing genetic factors of XFG could be used to predict the risk of developing the disease prior to onset in order to stop, or at least hinder, the irreversible progression toward blindness by initiating early medical intervention.

In 2007, Thorleifsson *et al.* reported a genome-wide association study (GWAS) using the populations from Iceland and Sweden, and described that one intronic variant and two nonsynonymous coding variants of lysyl oxidase-like 1 gene (*LOXL1*) confer the risk of developing XFG, possibly through XFS[5]. From the functional point of view, the involvement of *LOXL1* in XFG pathogenesis is quite rational, because *LOXL1* plays an indispensable role in elastic fiber homeostasis and maintaining the structures of the trabecular meshwork, the tissue that determines the IOP level in the eye[6]. However, *LOXL1*, in and of itself, fails to sufficiently explain the complex mechanism of the disease progression of XFG through XFS. This observation is also supported from the point of view of genetics, as many replication studies using populations derived from different genetic backgrounds

(Caucasians from the US[7–9] and Europe[10,11], Asians from Japan[12–16] and China[17,18], and Africans from South Africa[19]) have succeeded in replicating the association of the *LOXL1* variants, although the allele frequency of the variants varied among the ethnicities. In fact, the risk allele of one of the exonic variants (rs1048661) has been found to be inverted between Japanese[12] and Nordic populations[5]. Consequently, it is wise to investigate other modifying or causative variants in genes other than *LOXL1* by performing a GWAS using a non-Caucasian population in order to identify variants that are determining the different etiology of XFS onset and its progression to XFG among the ethnicities.

In this present study, we conducted a GWAS and replication study using two independent populations of Japanese case-control subjects in an attempt to identify new variants associated with XFS/XFG. As a result, we identified a cluster of genome-wide significant SNPs only from the chromosome 15q24.1, which is well known as a locus including *LOXL1*[5]. However, the genome-wide significant SNPs were distributed in not only *LOXL1*, but also in the two adjacent genes, *TBC1D21* and *PML*, without being in significant linkage disequilibrium (LD). We also identified a suggestive association only between *TBC1D21* and *LOXL1* variants by a conditional analysis, and revealed a unique haplotype structure of the variants derived from these two genes in our study population. Together with the accumulating knowledge of *LOXL1*-XFS/XFG relationships, the variants and genes newly discovered in this study would help to provide a better prediction of XFG risk assessment, as well as to elucidate the molecular mechanism of XFG pathogenesis through XFS.

## Results

**GWAS for XFS/XFG.** The samples used in this study are summarized in Table 1. In order to perform GWAS, we first selected the XFS/XFG subjects based on our strict diagnosis criteria, and then obtained the genotype data. We performed a GWAS using a population consisting of 201 XFS/XFG patients and 697 healthy controls (Table 1). In total, 652,792 SNPs that passed the quality controls (QC) were used for the association study (Figure 1A). According to the quantile-quantile (Q-Q) plot (Supplementary Material, Figure S1), the genomic inflation factor ($\lambda$) showed 1.020, suggesting that the population substructure should not have any substantial effects on the association analysis. Under those conditions, we observed a strong association signal from a locus on chromosome 15 (Figure 2A). In fact, we obtained 34 genome-wide significant SNPs (Supplementary Material, Table S1) that passed the Bonferroni correction threshold ($0.05/652{,}792 = 7.66 \times 10^{-8}$) on chromosome 15q24.1 (Figure 2A). Surprisingly, these significant SNPs were found to be broadly distributed in not only *LOXL1*, but also the adjacent two genes, *TBC1D21* and *PML*. The significance for this region was also confirmed by an imputation analysis (Figure 2B). According to the LD plots (Supplementary Material, Figure S2A), the SNPs in each gene seemed to be derived from 3 distinct LD blocks, which was also confirmed by the LD values using 34 genome-wide significant SNPs (Supplementary Material, Table S2).

Table 1 | Sample Information

| Study | Group | Subgroup | n | Age | F/M |
|---|---|---|---|---|---|
| GWAS | XFS/XFG[a] | Total | 201 | 74.3 ± 8.9 | 0.9 |
| | | XFG | 162 | 75.3 ± 8.5 | 0.8 |
| | | XFG with other glaucoma | 21 | 72.3 ± 10.5 | 0.9 |
| | | XFS | 18 | 66.8 ± 6.6 | 3.5 |
| | Control | Total | 697 | 58.5 ± 13.4 | 1.9 |
| Replication | XFS/XFG[b] | Total | 121 | 74.7 ± 8.6 | 1.0 |
| | | XFG | 103 | 75.8 ± 7.9 | 0.8 |
| | | XFG with other glaucoma | 18 | 68.4 ± 9.8 | 2.6 |
| | Control | Total | 263 | 48.6 ± 14.8 | 1.5 |

[a]Ninety XFG and 2 XFG with other glaucoma samples are overlapped with our previous study[12].
[b]One XFG sample is overlapped with our previous study[12].

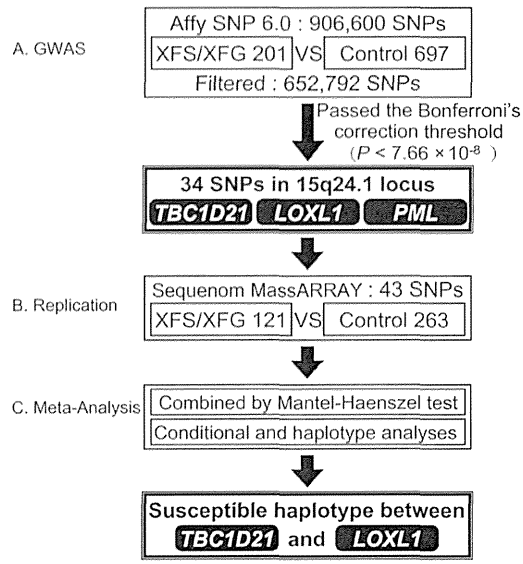


**Figure 1 | Study design.** (A) First, a GWAS was performed and 652,792 SNPs were analyzed for 201 XFS/XFG patients and 697 controls. As a result, 34 genome-wide significant SNPs were obtained from the genes of *TBC1D21*, *LOXL1*, and *PML* at15q24.1 locus. (B) Next, the GWAS results were replicated by analyzing 43 SNPs from the 15q24.1 locus by using an independent population of 121 XFS/XFG patients and 263 controls. (C) Finally, a meta-analysis was performed by combining the two data sets by use of the Mantel-Haenszel test. In addition, the pairs of significant SNPs were assessed by conditional and haplotype analyses. The result suggested the susceptible haplotype might exist for XFS/XFG from *TBC1D21* and *LOXL1* variants.

**Replication study.** Next, we attempted to replicate the GWAS results by analyzing an independent Japanese population consisting of 121 XFS/XFG patients and 263 controls (Table 1). We assessed a total of 43 SNPs at 15q24.1 locus, including 34 genome-wide significant SNPs from our GWAS results and 2 nonsynonymous coding SNPs (cSNPs) (rs1048661 and rs3825942) in exon 1 of *LOXL1* that reportedly are strongly associated with XFS/XFG[5]. As a result, almost every genome-wide significant SNP, except 1 SNP (rs723434), passed the Bonferroni correction threshold in the replication study ($0.05/43 = 1.16 \times 10^{-3}$) (Supplementary Material, Figure S2B and Table S3), confirming the association results obtained by GWAS. We also confirmed the association result of the reported 2 cSNPs in *LOXL1* using our Japanese population, of which the risk allele of rs1048661 was indeed inverted from the reported result with Caucasian. When the combined *P* values of GWAS and the replication study were calculated by use of the Mantel-Haenszel test[20], the level of significance of almost every SNP increased. In fact, rs893818, which was the most significant SNP in intron 1 of *LOXL1*, reached to $P = 8.21 \times 10^{-84}$ (Supplementary Material, Figures S2C and S2D, Table S4). The rs893818 SNP was clearly independent from the SNPs in *TBC1D21* and *PML* as in reference to the LD values calculated by applying the whole samples used in this study (Supplementary Material, Table S2). Moreover, the LD blocks based on the whole samples demonstrated that *LOXL1*, *TBC1D21*, and *PML* were in 3 distinct LD blocks, suggesting that the variants from different genes were independently contributing to the disease (Supplementary Material, Figures S2E and S2F).

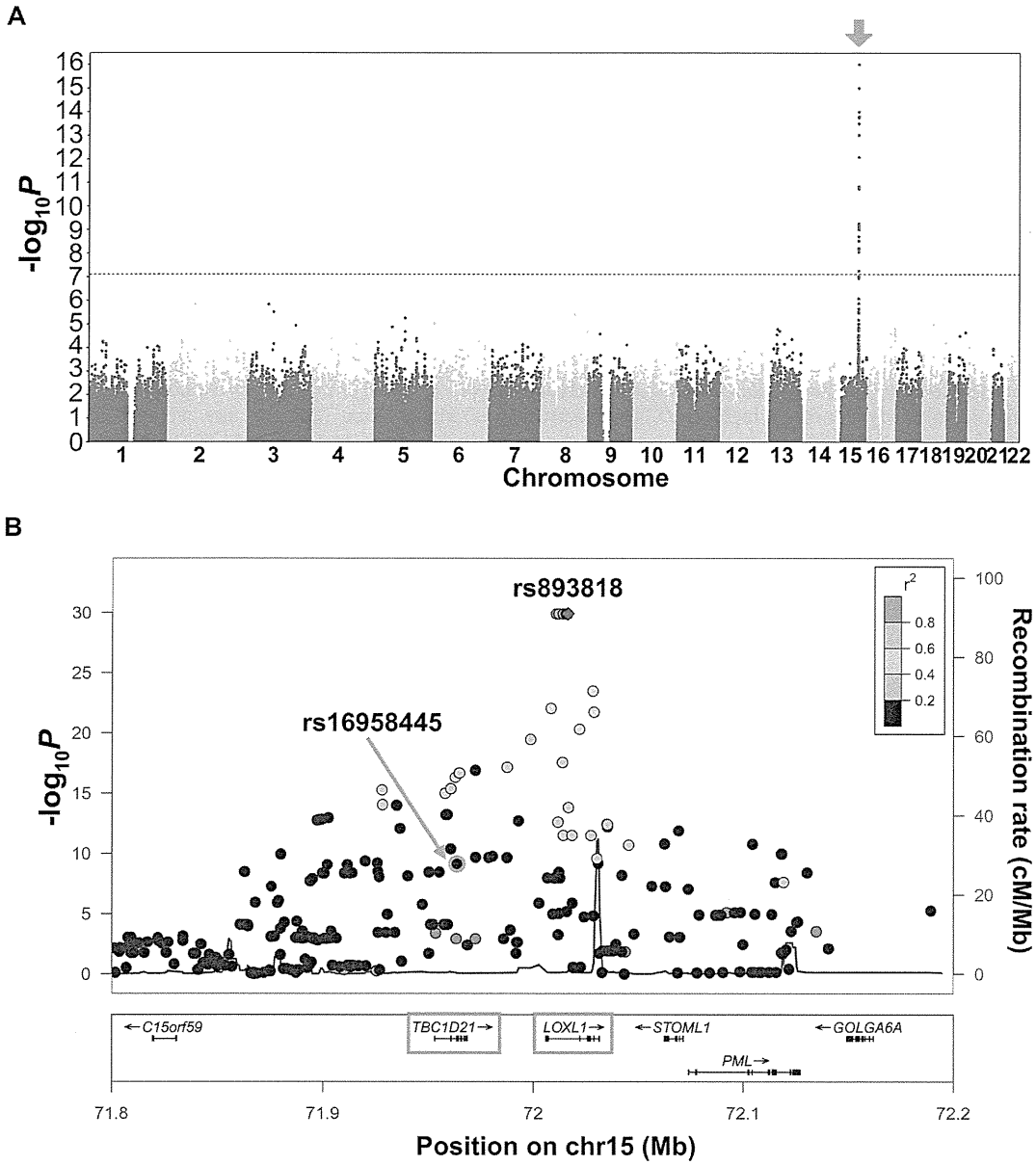


**Figure 2 | Association results.** (A) The SNPs with a strong association signal from the GWAS result appeared to exist as a cluster on chromosome 15 (red arrow). Horizontal dotted line represents Bonferroni correction threshold ($P < 7.66 \times 10^{-8}$). (B) Because the genome-wide significant SNPs were intensively identified on the 15q24.1 locus, we also imputed the SNPs across the locus and plotted against the positions based on the NCBI Build 36 coordinates. The LD value of $r^2$ is referred to the most significant SNP (rs893818) in the GWAS. The cSNP (rs16958445) and two genes (*TBC1D21* and *LOXL1*) used in the conditional and haplotype association analyses are highlighted by red. The genetic recombination rates (cM/Mb) estimated by HapMap Project[31] in Release 22 are indicated by the thin blue line.

**Meta-analysis of two studies.** We then performed a conditional analysis for 34 genome-wide significant SNPs on the basis of rs893818 according to our GWAS result. Overall, it turned out that the effect of rs893818 was very strong, while the variants in *TBC1D21* and *PML* were generally weak, although we found a suggestive signal ($P = 0.027$) from a nonsynonymous variant in exon 4 of *TBC1D21* (rs16958445) (Supplementary Material, Table S5). These two SNPs were considered to be truly associated with XFS/XFG because there were no confounding factors such as age and gender (Supplementary Material, Table S6). Consequently, we obtained 3 susceptible cSNPs, including 2 reported cSNPs in *LOXL1*, showing a weak correlation ($r^2 < 0.2$) to each other (Supplementary Material, Figures S3). Therefore, we then evaluated the combinational effect of 3 cSNPs (rs16958445 from *TBC1D21*, and rs1048661 and rs3825942 from *LOXL1*) in order to analyze the susceptibility to XFS/XFG by performing a haplotypic association analysis with the samples used in the replication study (Table 2). As a result, haplotype H6 (rs16958445: G, rs1048661: T, and rs3825942: G) was most significant for the association with XFS/XFG. Interestingly, haplotype H6 was more significant than haplotypes H3 and H4, including the significant haplotype (rs1048661: G and rs3825942: G) in the *LOXL1* for the Caucasian population[5]. In addition, according to the dbSNP database, rs16958445 in *TBC1D21* was found to be monomorphic for the G allele in Caucasian and

Table 2 | Results of Haplotype Association Analysis

| Haplotypes | SNP alleles[a] | Freq. in XFS/XFG | Freq. in controls | Chi-square | *P*-values[b] |
|---|---|---|---|---|---|
| | OMNIBUS | NA | NA | 122.4 | $9.57 \times 10^{-25}$ |
| H1 | GGA | 0.0039 | 0.1294 | 31.9 | $1.62 \times 10^{-8}$ |
| H2 | GTA | 0.0043 | 0.0407 | 7.7 | 0.0055 |
| H3 | AGG | 0.0176 | 0.0835 | 12.2 | 0.0005 |
| H4 | GGG | 0.0125 | 0.1517 | 33.4 | $7.55 \times 10^{-9}$ |
| H5 | ATG | 0.0319 | 0.0675 | 3.9 | 0.0471 |
| H6 | GTG | 0.9297 | 0.5272 | 118.5 | $1.33 \times 10^{-27}$ |

[a]Haplotypes were constructed with the SNPs in the following order: rs16958445, rs1048661, and rs3825942.
[b]*P* values were calculated by use of the 'hap-assoc' option of PLINK.

African populations. Consequently, we obtained a unique haplotype structure in this present study showing a high XFS/XFG susceptibility specific for the Asian population.

Taken together, the newly identified genes in 15q24.1 locus, together with the unique haplotype of *TBC1D21* and *LOXL1* variants, could add some information to explain the molecular mechanism of XFS/XFG pathogenesis, which has been considered difficult to explain by *LOXL1* alone.

## Discussion

In this study, we successfully obtained the genetic markers strongly associated with XFS/XFG patients by analyzing two independent Japanese populations totaling 1,282 subjects from GWAS and its replication study. As a result, we discovered the genome-wide significant variants in not only *LOXL1*, but also 2 other genes, *TBC1D21* and *PML*, both of which are located on chromosome 15q24.1, which is well known as the "*LOXL1* locus"[5]. We also found a suggestive combinational effect of the variants related to the XFS/XFG susceptibility only between *LOXL1* and *TBC1D21*, which seemed to be specific to Asian population.

In the first reported GWAS for XFS/XFG, Thorleifsson *et al.* detected a strong association signal only in *LOXL1* at the 15q24.1 locus from a Nordic population[5]. Their GWAS was carried out based on the genotype data generated by using the Infinium HumanHap300 BeadChip (Illumina, Inc., San Diego, California, USA) array, whereas we used the Genome-Wide Human SNP Array 6.0 (SNP 6.0; Affymetrix, Inc., Santa Clara, California, USA), in which the SNP coverage is more than three-fold. We precisely compared the probe disposition derived from each microarray as well as the association results from the two studies across the locus (Supplementary Material, Figure S4A and B). Although the number of QC-passed SNPs in the locus was different in the two studies depending on which microarrays and sample ethnicities were used, we were able to directly compare the results for some SNPs (Supplementary Material, Figure S4A; connected with green lines). As a result, a genome-wide significant SNP in *LOXL1* was reproducible in both studies. However, the genome-wide significant SNPs in other genes at the 15q24.1 locus, especially in *TBC1D21* (Supplementary Figure S4B), obtained in our study using Japanese samples were not significant in the first reported GWAS using the Caucasian samples. Moreover, we found that 1 of the significant SNPs in *TBC1D21*, rs16958445, which together with 2 cSNPs in *LOXL1* seemed to be contributing to the disease according to the results of the conditional analysis, was a monomorphic SNP in all of the HapMap populations other than Asian (see dbSNP in NCBI).

With regard to rs16958445, the non-risk allele "A" was a minor allele, whose frequency was about 0.144–0.157 or 0.166 in Japanese, according to the dbSNP or our control samples, respectively (Supplementary Material, Table S4). This meant that the contribution of rs16958445 to the XFS/XFG susceptibility might be limited for explaining the different susceptibility among the ethnicities. However, the results of the haplotype association analysis by 3 cSNPs (H6: GTG in Table 2) demonstrated that the significance was higher than that by use of only 2 cSNPs in *LOXL1* (Supplementary Material, H4: TG in Table S7). In addition, the non-risk allele of rs16958445 decreased the significance of the major susceptible haplotype in Caucasians (Supplementary Material, H3: GG in Table S7). Taken all together, we concluded that the discrepancy of the results from the two studies was due to the different genetic backgrounds of the samples, and not due to practical reasons such as the microarray density.

The association results of *LOXL1* variants found in the Nordic population has been extensively characterized in many other populations with different ethnic backgrounds. In particular, out of the three variants reported, two coding variants of rs1048661 (Arg141Leu) and rs3825942 (Gly153Asp) in exon 1 were mostly analyzed by the replication analysis[21] (Supplementary Material, Figure S5). Although both of the variants were found to be associated with the disease broadly beyond the ethnicities, the risk alleles of rs1048661 and rs3825942 were, intriguingly, inverted in Japanese[12]/Chinese[18] and South African[19] populations, respectively. The inverted genotypes of the risk alleles among different populations may be reflecting the different patterns of historical recombination between these SNPs and the unidentified causative variants. However, the one thing that is apparent is that the particular amino-acid changes in LOXL1 protein were not functionally sufficient enough to be the causative factor for the disease pathogenesis. Consequently, it would have been wise to investigate other modifying or causative variants in genes other than *LOXL1*. Thus, we decided to perform a GWAS using our Japanese population in order to identify unique variants contributing to the onset of XFS and its progression to XFG.

To date, only a limited number of disease-associated variants identified by GWAS were applicable to the actual diagnosis in the clinic setting. Thus far, a case in point is the diagnosis that has been applied to predict the risk of age-related macular degeneration (AMD)[22,23]. In order to predict the prevalence and incidence of AMD, multiple risk models have been developed by incorporating both the genetic and environmental factors, resulting in a marked increase of the accuracy to discriminate risk and non-risk individuals[24]. However, in the case of XFS/XFG, the situation is completely different from that of AMD, due to the limited number of identified genetic factors as well as their characteristics. Although the prevalence of *LOXL1* variants in affected patients is strikingly high (>80%), which means that the sensitivity is high, the prevalence of unaffected controls is also high enough (up to 88%) to render the specificity being low, indicating that the simple allelic testing of *LOXL1* variants themselves cannot exclude the individuals who would not develop XFS/XFG[21]. Although the variants identified in this study seemed to possess a weaker effect on the disease than the *LOXL1* variants have, we also discovered a unique haplotype specific for the Japanese population (Table 2). Combining the information of each allele and the haplotypes would help in developing a better diagnosis to predict XFS/XFG risk by the genetic testing of these variants.

Since XFS is characterized by clinically visible abnormal fibrillar deposits (i.e., PEX), progressive accumulation of those deposits have been considered to be a trigger of developing glaucoma by increasing the outflow resistance of the trabecular meshwork, resulting in the continuous elevation of IOP[3]. The LOXL1 protein, which catalyzes the formation of elastin fibers and contributes to the trabecular meshwork structures, is thus probably involved in the XFS/XFG pathogenesis[6]. However, the exonic variants in *LOXL1* fail to sufficiently explain the complex mechanism of the disease (e.g., as if they were affecting the quality (amino-acid changes) and/or quantity (expression level) of LOXL1 protein) due to the differences in allelic distribution among different genetic backgrounds and the high prevalence of the variants in the healthy population[21].

According to our GWAS result, the significant variants for XFS/XFG other than the *LOXL1* variants were newly discovered from *TBC1D21* and *PML* genes (Figure 2B, Supplementary Material, Figure S2). In fact, the *TBC1D21* gene, which belongs to the TBC1 domain family, was suggested to be related to *LOXL1* by haplotype association analysis (Table 2). The TBC (Tre-2/Bub2/Cdc16) domain consists of approximately 200 amino acids and is considered to function as a GTPase activator of Rab proteins. However, the functional details of more than 40 members of the protein families in humans and mice, including *TBC1D21*, have to date not been well investigated[25]. Although there are few functional analyses of the gene, our RT-PCR analysis revealed that *TBC1D21* is expressed in the human retina (Supplementary Material, Figure S6). When we compared the sequence conservation of the variant (rs16958445) among several species, we found that the variant was conserved within primates (Supplementary Material, Figure S7). We also performed *in silico* prediction in order to evaluate the influence of amino acid change in rs16958445 by means of SIFT[26] and PolyPhen-2[27], and programs predicted as "TOLERATED" and "benign", respectively. The results suggested that the amino acid change in rs16958445 does not affect the function of TBC1D21 protein. Consequently, further functional investigation is necessary to elucidate whether or not *TBC1D21* involves in the disease etiology of XFS/XFG.

On the other hand, *PML* is functionally well characterized and would be a good target for analyzing the relationship to XFS/XFG etiology, although the contribution to XFS/XFG susceptibility was considered to be marginal than *TBC1D21* and *LOXL1* based on our analysis. *PML* is a member of the tripartite motif (TRIM) family and famous for being involved in generating fusion protein as a result of chromosomal translocation with the retinoic acid receptor alpha gene, which is often associated with acute promyelocytic leukemia[28]. The original function of PML protein is to form a nuclear body, which carries several components, such as pRB, p53, CBP, elf-4, Daxx, SUMO-1, etc[29]. Therefore, if the variants in *PML* cause inappropriate formation of the nuclear body, broad biological functions would be affected, including transcriptional regulation, initiation of translation, and sumoylation, which could associate with the elastic microfibrillopathy. In fact, our RT-PCR analysis shows that *PML* is expressed in the human retina (Supplementary Material, Figure S6). Consequently, we consider that it would be interesting to further investigate the involvement of *PML* in the XFS/XFG pathogenesis.

Although we succeeded in obtaining some new variants and genes associated with XFS/XFG, it should be noted that there must be other gene(s) in other region(s) contributing to the disease in order to explain the complex mechanism of XFS/XFG pathogenesis. Moreover, under the current GWAS condition, we are unable to verify whether or not the variants were specifically related to the mechanism for the progression to glaucoma from XFS. Since there are patients who possess PEX, but never develop glaucoma, other factors must be involved in determining whether or not XFS patients develop glaucoma. Together with the variants/genes identified in this study and the accumulated knowledge of *LOXL1*, the identification of the remaining variants as well as the variants specific for XFS patients without glaucoma could provide a complete set of genetic factors associated with XFS and XFG, which should be useful for their diagnostic tools as well as for revealing the molecular mechanism of their etiology.

## Methods

**Subjects.** All of the procedures in this study were performed in accordance with the tenets set forth in the Declaration of Helsinki and were approved by the Institutional Review Board of Kyoto Prefectural University of Medicine, Kyoto, Japan. Written informed consent was obtained from all XFS/XFG participants after receiving a detailed and thorough explanation of the study. Those participants were interviewed to determine their familial history of glaucoma and the medical histories of other ocular or general diseases. The Japanese volunteers were recruited between March 2005 and August 2012 at the University Hospital of Kyoto Prefectural University of Medicine in order to provide peripheral blood samples. The genotyping data of this current study for XFS/XFG patients and healthy volunteers was simultaneously obtained with the data of our previous study for POAG[30]. From the complete data set, XFS/XFG cases and controls suitable for this study were selectively chosen from the complete data set based on the following strict diagnosis: 1) all XFG patients were diagnosed by slit-lamp examination for the existence of exfoliation materials on the pupil and surface anterior lens capsule with open angle, 2) IOP higher than 21 mmHg, and 3) visual field defect according to the optic nerve appearance. The category "XFG with other glaucoma" group includes normal tension glaucoma or primary angle closure glaucoma with XFS. All of the patients and healthy volunteers were diagnosed by 3 ophthalmologists (Y.I., M.U., and K.M.) from a single institution. The demographics (i.e., subject age and male-to-female ratio) of all of the subjects used in this study are shown in Table 1. To examine the possible confounding effects of the age and gender of the subjects, correlations between the case and control samples were assessed by use of the Student's *t* test or chi-square test (Table 1).

**SNP genotyping and quality control for the GWAS.** As described previously[30], 906,600 SNPs were genotyped for 2,126 Japanese subjects including POAG patients, XFS/XFG patients, and healthy volunteers by Genome-Wide Human SNP Array 6.0 (Affymetrix), and strict QC was applied. For the GWAS, 203 XFS/XFG patients and 718 controls were initially selected from the total number of subjects based on the latest diagnosis. In order to exclude subjects within the population who were genetically related, identity-by-descent estimates were performed for all possible combinations by PLINK v1.07 (see URLs). As a result, 2 XFS/XFG patients and 21 controls who were assumed to be genetically related were excluded from the GWAS population. Ultimately, the population ended up with 201 XFS/XFG patients and 697 controls (Figure 1A and Table 1). Population stratification was examined by principal component analysis using EIGENSTRAT software v3.0 (see URLs). The four HapMap populations (CEU, YRI, JPT, and CHB) were simultaneously applied into EIGENSTRAT as the reference. The generated cluster plots indicated that the XFG and control population were genetically clustered within the JPT population, and there was no outlier sample (Supplementary Material, Figure S8). In order to extract high-quality autosomal SNP genotype data, the following QC filters were applied: (i) call rate per SNPs in each case and control samples $\geq$95%, respectively, (ii) minor allele frequency (MAF) in case and control samples $\geq$1%, and (iii) Hardy-Weinberg equilibrium (HWE) in control samples with a *P*-value $\geq$0.001. Consequently, the remaining 652,792 SNPs were analyzed for the XFS/XFG GWAS (Figure 1A).

**Replication study.** For the replication study, an independent population of 384 samples consisting of 121 XFS/XFG patients and 263 controls was prepared (Table 1). Those samples were extensively checked in order to remove any familial relationships. In total, 41 SNPs were applied to the replication by referencing the GWAS results as follows: 34 SNPs that passed the Bonferroni's correction in our GWAS and 7 SNPs which were selected to be useful for confirming the LD region of 15q24.1 locus. In addition, 2 cSNPs (rs1048661 and rs3825942) were assessed that have been reported by Thorleifsson *et al.*[5], yet are not designed in SNP 6.0. Furthermore, 4 SNPs associated with POAG in our previous study[30] were included in this replication assay. In total, 47 SNPs were divided into each of the two groups of 30 and 17 SNPs per assay plate, respectively, according to the manufacturer's recommendation, and genotyped simultaneously for 384 samples in each group by use of the MassARRAY iPLEX Genotyping system (Sequenom, Inc., San Diego, California, USA). All of the resulting call rates of these SNPs were over 90%.

**Meta-analysis.** A meta-analysis was performed for 41 SNPs, which were genotyped in both the GWAS and replication study, by use of the Mantel-Haenszel test[20]. Among these SNPs, rs2165241 and rs4243042 were found to be monomorphic for the XFS/XFG subjects used in the replication study (i.e., the risk allele frequency was 100%). Therefore, those 2 SNPs were excluded from the Mantel-Haenszel test. Genotype imputation for GWAS was performed using MACH ver. 1.0.16 software (see URLs). The genotype data of JPT and CHB in the HapMap Phase 2[31] (release #24) were applied as the reference for haplotyping. After the QC was applied for the imputation results (MAF $\geq$0.01 and *Rsq* $\geq$0.7), association analysis of the SNPs for XFS/XFG was performed by use of mach2dat ver. 1.1.9 software (Windows version). Conditional analysis was assessed for 34 genome-wide significant SNPs using the combined samples from the GWAS and the replication study (i.e., 322 XFS/XFG patients and 960 controls). Haplotype analysis was examined with the samples from the

replication study in order to assess the reported cSNPs in *LOXL1*. Both conditional and haplotype analyses were performed by use of the PLINK v1.07 whole genome association analysis toolset.

**Data management and statistical analysis.** In order to manage and analyze all of the genotype data, our in-house Genoika Server System[30,32,33] was used. The Genoika Server System comes with PLINK, R program with some packages, EIGENSTRAT, and Haploview (see URLs for the details of each software) built in, and all of the analyses were performed by use of this system. In addition, Microsoft Office Excel 2003 (Microsoft Corporation, Redmond, Washington, USA) was used for preparing the data sets and statistical analysis. The frequency of alleles in the case and control samples was compared by use of the basic allele test. The odds ratio (OR) and the upper and lower limit of the 95% confidence interval (CI) of each SNP were calculated for the allele possessing a higher frequency in the case samples than in the control samples. The HWE was evaluated by use of the chi-square test. A regional plot in Figure 2 was drawn by use of LocusZoom ver. 1.1 (see URLs) genetic analysis software. Q-Q plots were generated by ranking the observed values from minimum to maximum and plotting them against their expected chi-square values using the "snpStats" package ver. 1.10.0 in the R program (see URLs).

**URLs.** PLINK software v1.07, http://pngu.mgh.harvard.edu/~purcell/plink/; EIGENSTRAT software v3.0, http://genetics.med.harvard.edu/reich/Reich_Lab/Welcome.html; MACH ver. 1.0.16 and mach2dat ver. 1.1.9 softwares, http://www.sph.umich.edu/csg/abecasis/MACH/index.html; Haploview v4.2, http://www.broadinstitute.org/scientific-community/science/programs/medical-and-population-genetics/haploview/haploview; LocusZoom version 1.1, http://csg.sph.umich.edu/locuszoom/. R programs, http://www.r-project.org/; SIFT dbSNP DB (build 132), http://sift.jcvi.org/; PolyPhen-2 version 2.2.2 r398, http://genetics.bwh.harvard.edu/pph2/.


1. Quigley, H. A. & Broman, A. T. The number of people with glaucoma worldwide in 2010 and 2020. *Br J Ophthalmol* **90**, 262–7 (2006).
2. Kwon, Y. H., Fingert, J. H., Kuehn, M. H. & Alward, W. L. Primary open-angle glaucoma. *N Engl J Med* **360**, 1113–24 (2009).
3. European Glaucoma Society. Terminology and guidelines for glaucoma, 3rd Edition. (Dogma, Savona, Italy, 2008).
4. Iwase, A. *et al.* The prevalence of primary open-angle glaucoma in Japanese: the Tajimi Study. *Ophthalmology* **111**, 1641–8 (2004).
5. Thorleifsson, G. *et al.* Common sequence variants in the LOXL1 gene confer susceptibility to exfoliation glaucoma. *Science* **317**, 1397–400 (2007).
6. Schlotzer-Schrehardt, U. Molecular pathology of pseudoexfoliation syndrome/glaucoma--new insights from LOXL1 gene associations. *Exp Eye Res* **88**, 776–85 (2009).
7. Fingert, J. H. *et al.* LOXL1 mutations are associated with exfoliation syndrome in patients from the midwestern United States. *Am J Ophthalmol* **144**, 974–975 (2007).
8. Challa, P. *et al.* Analysis of LOXL1 polymorphisms in a United States population with pseudoexfoliation glaucoma. *Mol Vis* **14**, 146–9 (2008).
9. Fan, B. J. *et al.* DNA sequence variants in the LOXL1 gene are associated with pseudoexfoliation glaucoma in a U.S. clinic-based population with broad ethnic diversity. *BMC Med Genet* **9**, 5 (2008).
10. Pasutto, F. *et al.* Association of LOXL1 common sequence variants in German and Italian patients with pseudoexfoliation syndrome and pseudoexfoliation glaucoma. *Invest Ophthalmol Vis Sci* **49**, 1459–63 (2008).
11. Mossbock, G. *et al.* Lysyl oxidase-like protein 1 (LOXL1) gene polymorphisms and exfoliation glaucoma in a Central European population. *Mol Vis* **14**, 857–61 (2008).
12. Mori, K. *et al.* LOXL1 genetic polymorphisms are associated with exfoliation glaucoma in the Japanese population. *Mol Vis* **14**, 1037–40 (2008).
13. Hayashi, H., Gotoh, N., Ueda, Y., Nakanishi, H. & Yoshimura, N. Lysyl oxidase-like 1 polymorphisms and exfoliation syndrome in the Japanese population. *Am J Ophthalmol* **145**, 582–585 (2008).
14. Ozaki, M. *et al.* Association of LOXL1 gene polymorphisms with pseudoexfoliation in the Japanese. *Invest Ophthalmol Vis Sci* **49**, 3976–80 (2008).
15. Mabuchi, F. *et al.* Lysyl oxidase-like 1 gene polymorphisms in Japanese patients with primary open angle glaucoma and exfoliation syndrome. *Mol Vis* **14**, 1303–8 (2008).
16. Fuse, N. *et al.* Evaluation of LOXL1 polymorphisms in eyes with exfoliation glaucoma in Japanese. *Mol Vis* **14**, 1338–43 (2008).
17. Lee, K. Y. *et al.* Association of LOXL1 polymorphisms with pseudoexfoliation in the Chinese. *Mol Vis* **15**, 1120–6 (2009).
18. Chen, L. *et al.* Evaluation of LOXL1 polymorphisms in exfoliation syndrome in a Chinese population. *Mol Vis* **15**, 2349–57 (2009).
19. Williams, S. E. *et al.* Major LOXL1 risk allele is reversed in exfoliation glaucoma in a black South African population. *Mol Vis* **16**, 705–12 (2010).
20. Mantel, N. & Haenszel, W. Statistical aspects of the analysis of data from retrospective studies of disease. *J Natl Cancer Inst* **22**, 719–48 (1959).
21. Challa, P. Genetics of pseudoexfoliation syndrome. *Curr Opin Ophthalmol* **20**, 88–91 (2009).
22. Klein, R. J. *et al.* Complement factor H polymorphism in age-related macular degeneration. *Science* **308**, 385–9 (2005).
23. Maller, J. *et al.* Common variation in three genes, including a noncoding variant in CFH, strongly influences risk of age-related macular degeneration. *Nat Genet* **38**, 1055–9 (2006).
24. Chen, Y., Bedell, M. & Zhang, K. Age-related macular degeneration: genetic and environmental factors of disease. *Mol Interv* **10**, 271–81 (2010).
25. Fukuda, M. TBC proteins: GAPs for mammalian small GTPase Rab? *Biosci Rep* **31**, 159–68 (2011).
26. Kumar, P., Henikoff, S. & Ng, P. C. Predicting the effects of coding non-synonymous variants on protein function using the SIFT algorithm. *Nat Protoc* **4**, 1073–81 (2009).
27. Adzhubei, I. A. *et al.* A method and server for predicting damaging missense mutations. *Nat Methods* **7**, 248–9 (2010).
28. de The, H. & Chen, Z. Acute promyelocytic leukaemia: novel insights into the mechanisms of cure. *Nat Rev Cancer* **10**, 775–83 (2010).
29. Zhong, S., Salomoni, P. & Pandolfi, P. P. The transcriptional role of PML and the nuclear body. *Nat Cell Biol* **2**, E85–90 (2000).
30. Nakano, M. *et al.* Common variants in CDKN2B-AS1 associated with optic-nerve vulnerability of glaucoma identified by genome-wide association studies in Japanese. *PLoS One* **7**, e33389 (2012).
31. International HapMap, C. *et al.* A second generation human haplotype map of over 3.1 million SNPs. *Nature* **449**, 851–61 (2007).
32. Nakano, M. *et al.* Three susceptible loci associated with primary open-angle glaucoma identified by genome-wide association study in a Japanese population. *Proc Natl Acad Sci U S A* **106**, 12838–42 (2009).
33. Ueta, M. *et al.* Association between prostaglandin E receptor 3 polymorphisms and Stevens-Johnson syndrome identified by means of a genome-wide association study. *J Allergy Clin Immunol* **126**, 1218-25 e10 (2010).


## Acknowledgments

The authors wish to thank all the patients and volunteers who enrolled in the study. We also thank Professor T. Miki for managing the anonymous code-assignment process; S. Ohashi, M. Yamashita, and N. Saito for processing blood samples and performing genotyping; H. Yamada for the assistance in clinical information analysis; F. Sato for the management of genotype data and building the analyzing system; T. Ichikawa for excellent secretarial assistance; and J. Bush for reviewing the manuscript. This work was supported by the grants from the Takeda Science Foundation to MN, the Collaborative Development of Innovative Seeds of Japan Science and Technology Agency (JST) to MK and KT, the Ministry of Health, Labor and Welfare of Japan to MN, KM, SK and KT, and Santen Pharmaceutical Co. Ltd. to SK and KT.

## Author contributions

Designed the research: M.K., S.K. and K.T. Performed the research: M.N., Y.I., M.U., K.I., M.F., N.O., H.A. and K.M. Analyzed the data: M.N., Y.T., R.S. and M.F. Wrote the paper: M.N., Y.I., Y.T., K.M., S.K. and K.T. All authors reviewed the manuscript.

## Additional information

**Supplementary information** accompanies this paper at http://www.nature.com/scientificreports

**Competing financial interests:** This study has been completed under the Collaborative Research Agreement executed by Kyoto Prefectural University of Medicine and Santen Pharmaceutical Co., Ltd. All materials and information produced throughout this study are parts of co-owned intellectual properties. The authors MF and MK are employees of Santen Pharmaceutical Co., Ltd. All the other authors declare that no conflict of interest exists.

**How to cite this article:** Nakano, M. *et al.* Novel common variants and susceptible haplotype for exfoliation glaucoma specific to Asian population. *Sci. Rep.* **4**, 5340; DOI:10.1038/srep05340 (2014).

*Molecular Vision* 2014; 20:638-648 <http://www.molvis.org/molvis/v20/638>
Received 17 October 2013 | Accepted 11 May 2014 | Published 13 May 2014



# Three-dimensional architecture of collagen type VI in the human trabecular meshwork

**Elena Koudouna,[1] Robert D. Young,[1] Morio Ueno,[2] Shigeru Kinoshita,[2] Andrew J. Quantock,[1] Carlo Knupp[1]**

*[1]Structural Biophysics Group, School of Optometry and Vision Sciences, Cardiff University, Wales, UK; [2]Department of Ophthalmology, Kyoto Prefectural University of Medicine, Hirokoji Kawaramachi, Kyoto, Japan*

**Purpose:** Type VI collagen is a primary component of the extracellular matrix of many connective tissues. It can form distinct aggregates depending on tissue structure, chemical environment, and physiology. In the current study we examine the ultrastructure and mode of aggregation of type VI collagen molecules in the human trabecular meshwork.
**Methods:** Trabecular meshwork was dissected from donor human eyes, and three-dimensional transmission electron microscopy of type VI collagen aggregates was performed.
**Results:** Electron-dense collagen structures were detected in the human trabecular meshwork and identified as collagen type VI assemblies based on the three-dimensional spatial arrangement of the type VI collagen molecules, the 105-nm axial periodicity of the assemblies themselves, and their characteristic double bands, which arose from the globular domains of the type VI collagen molecules. Sulfated proteoglycans were also seen to associate with the assemblies either with the globular domain or the inner rod-like segments of the tetramers.
**Conclusions:** No extended structural regularity in the organization of type VI collagen assemblies within the trabecular meshwork was evident, and the lateral separation of the tetramers forming the assemblies varied, as did the angle formed by the main axes of adjacent tetramers. This is potentially reflective of the specific nature of the trabecular meshwork environment, which facilitates aqueous outflow from the eye, and we speculate that extracellular matrix ions and proteins might prevent a more tight packing of type VI collagen tetramers that form the assemblies.

Type VI collagen is a primary component of the extracellular matrix of many connective tissues [1,2], notably skin [3] and cornea. It was originally identified in pepsin fragments of human aortic intima [4] and designated as "intima collagen." After further electron microscopy and biochemical studies [3,5], intima collagen was renamed type VI collagen [6] and a detailed structural model for this type of collagen was proposed [7-13].

Type VI collagen is a heterotrimer and was long considered to be composed of three [14] genetically distinct alpha 1 (VI), alpha 2 (VI), and alpha 3 (VI) chains [15]. However, recently three novel collagen VI alpha chains have been discovered in humans: alpha 4 (VI), alpha 5 (VI), and alpha 6 (VI) chains [16,17]. After secretion into the extracellular matrix, the alpha chains assemble as type VI collagen molecules [5] that possess a central collagenous triple-helical segment, about 105 nm long, delimited at both ends by a globular domain (Figure 1A). Pairs of collagen VI molecules coil together in an antiparallel fashion [11] with a 30-nm axial shift to form dimers (Figure 1B) [5]. Two dimers associate laterally with no axial shift to give rise to a tetramer (Figure 1C) [6], which can be considered as the basic structural unit of collagen VI microfibrils (Figure 1D) [7,18]. Cysteine residues form disulfide bridges between monomers in dimers and between dimers in tetramers [19], and they stabilize the main collagen VI structural unit. Tetramers can be described as possessing an inner rod-like region and two outer rod-like regions separated by and ending with the collagen VI globular domains of the four molecules forming them (Figure 1C).

Unlike the more abundant type I collagen [3], type VI collagen gives rise to cross-banded aggregates that are characterized by a pattern of pairs of transverse bands approximately 30 nm apart with a periodicity of about 105 nm [6,9,18]. In particular, noncovalent bonds between the C- and N- terminal globular domains at each end [6] of the outer rod-like regions of two adjacent tetramers produce end-to-end, cross-banded, pseudofibrillar aggregates (Figure 1D) with a repeated ca. 30–75-nm spacing [5,20]. The same interactions between globular domains of the tetramers also account for the formation of more extended collagen VI aggregates [21] resembling open networks. The basic way in which collagen type VI tetramers can assemble explains the organization of morphologically distinct aggregates [22-24], which also depends on the structure and physiology of the tissue [25-28] in which they are found.

Correspondence to: Andrew Quantock, Structural Biophysics Group, School of Optometry and Vision Sciences, Cardiff University, Maindy Road, Cardiff CF24 4HQ, Wales, UK; Phone: +44 (0)29 20875064; FAX: +44 (0)29 20874859; email: address: QuantockAJ@cf.ac.uk

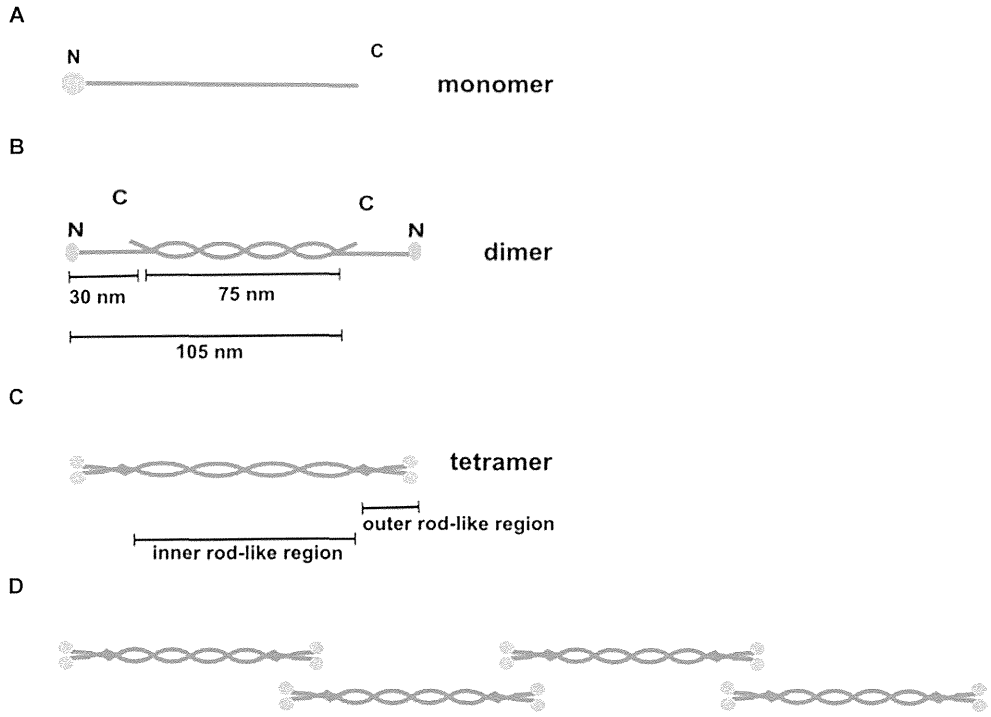


Figure 1. Schematic drawings of the structures of (**A**) monomer, (**B**) dimer, (**C**) tetramer, and (**D**) microfibrils of type VI collagen. N (NH2) and C (COOH) are the amino- and carboxy-terminal domains, represented in blue and yellow, respectively. The collagenous triple helices (red in color) associate laterally with a 30-nm axial shift in dimers (**B**). Pairs of dimers associate laterally to form tetramers (**C**). Tetramers can be described as possessing an inner rod-like region and two outer rod-like regions separated by and ending with the collagen VI globular domains. Limited resolution of collagen VI fibrils in micrographs causes the globular domains to appear as transverse electron-dense bands (**D**).

Type VI collagen interacts with extracellular matrix constituents [29,30] in several connective tissues [31-33]. Collagen type VI is associated with several human disorders. For example, individuals having Bethlem myopathy exhibit mutations of the collagen type VI genes (*COL6A1, COL6A2, COL6A3*) that affect the N- terminal domains [34-36]. Collagen type VI assemblies are also involved with pathogenesis of ocular disorders, including age-related macular degeneration [37] and Sorsby's fundus dystrophy [38]. Here, we examine the three-dimensional organization of collagen type VI aggregates in the human trabecular meshwork (Figure 2), the extracellular matrix of which provides flow resistance to aqueous humor leaving the anterior chamber of the eye [39] and which thus plays a role in the regulation of intraocular pressure.

## METHODS

*Specimen preparation and transmission electron microscopy:* Ocular tissues containing trabecular meshwork were dissected out by one of us (MU, an ocular surgeon) from both eyes of a 69-year-old female donor. Tissue, which was obtained from the Bristol Eye Bank, Bristol, UK, with full informed consent, was immediately fixed in 2.5% glutaraldehyde in 25 mM sodium acetate buffer (pH 5.7) containing 0.1 M $MgCl_2$ and 0.05% cuprolinic blue dye (the dye (Polysciences Inc., Warrington, PA) was included to stain sulfated proteoglycans). Samples were then washed in sodium acetate buffer to remove the glutaraldehyde fixative and cuprolinic blue dye. Immersion in 0.5% sodium tungstate was performed to add contrast to the stained proteoglycans, and dehydration was accomplished by exposing the tissue to a graded series of ethanol (50%–100%). Following conventional processing with epoxy resin embedding (Agar Scientific, Stansted, UK), ultrathin sections approximately 90 nm thick were cut on an Ultracut E ultramicrotome (Leica Microsystems (UK) Ltd, Milton Keynes, UK) and contrasted for transmission electron microscopy by staining with saturated aqueous uranyl acetate for 12 min followed by four washes in filtered distilled water (1 min per wash). Sections were examined with a JEOL 1010 transmission electron microscope (Jeol UK, Welwyn Garden City, UK) operating at 80 kV. Experiments were conducted in accordance with the ethical principles that have their origin in the Declaration of Helsinki and in line with the requirements of the UK Human Tissue Act.

*Electron tomography:* For electron tomography, 120-nm-thick sections were cut and collected on naked 200 mesh copper grids. After uranyl acetate staining as indicated above, 10 nm colloidal gold particles (BBI, Cardiff, UK) were deposited on both sides of the grid to serve as fiducial markers. A 92 single-axis tilt series of electron micrographs of collagen type VI assemblies was obtained from +60° to −60° in either 1° and 2° increments. Images were acquired using a Gatan

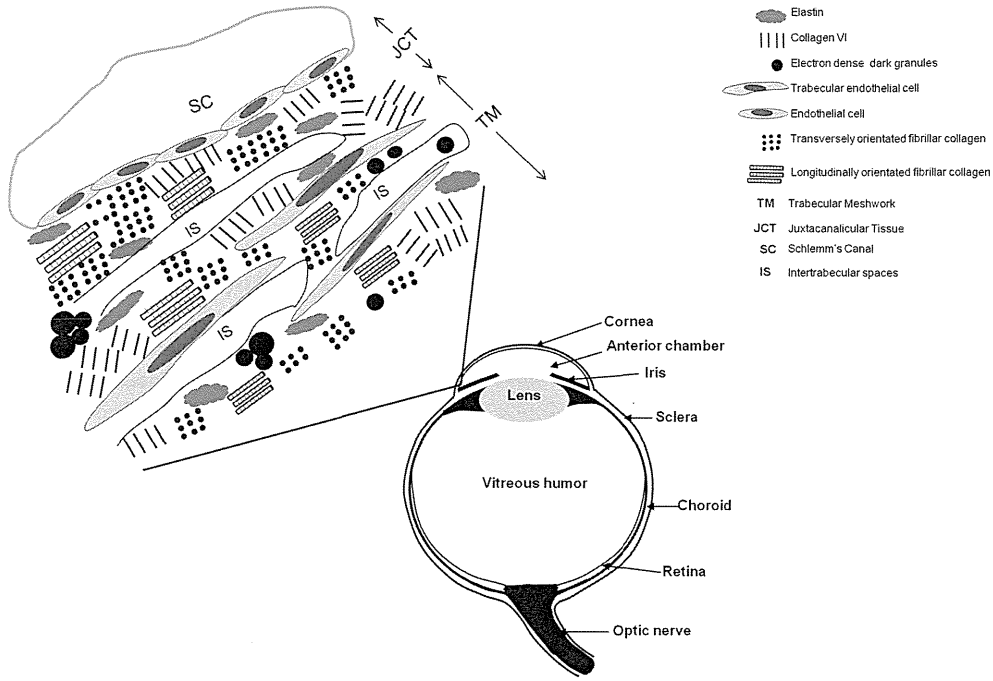


Figure 2. Schematic diagram of the eye showing the major ocular structures and the anatomic positions of the Schlemm's canal (SC), the juxtacanalicular tissue (JCT), and the trabecular meshwork (TM). The corneoscleral region of the TM is separated from SC by a connective tissue layer known as the JCT, which terminates adjacent to a layer of endothelial cells that line the inner wall of SC. The structure of the TM encompasses intertrabecular spaces (IS), trabecular sheets (trabecular beams) filled with extracellular matrix molecules, including elastin, collagens, some electron-dense dark granules, and thin trabecular endothelial cells. The IS as well as the trabecular sheets (trabecular beams) vary in size and shape.

ORIUS SC1000 charge coupled device camera (Gatan, Pleasanton, CA) at 20,000X magnification. Micrographs were aligned at a pixel size of 0.4 nm based on the position of the colloidal gold particles on each image. Tomographic reconstructions of longitudinal sections of trabecular meshwork type VI collagen aggregates and stained proteoglycan filaments were generated with the IMOD software package (Boulder, CO) [40]. Segmentation of the tomograms, three-dimensional analysis, and visualization were accomplished via the use of EM3D software (College Station, TX) [41]. Visualization of the reconstructed image stacks and the generation of animated stereo views were achieved with the 3DViewer plug-in of the ImageJ software package (Bethesda, MD) [42,43].

## RESULTS

Transverse, banded, collagenous assemblies were found to be widespread throughout the extracellular matrix of the human trabecular meshwork beams and the juxtacanalicular region. These assemblies, displaying an axial periodicity of 109±13 nm (mean±standard deviation, n=47), formed clusters of different sizes, which often lined the intratrabecular spaces and which were surrounded by interstitial collagen fibrils displaying the typical 67-nm axial periodicity (Figure 2 and Figure 3). These assemblies, from their general appearance and periodicity, closely resembled the assemblies of collagen VI molecules found in other tissues [21] and matched the 100–120-nm periodicity of presumed type VI collagen long-spacing collagen documented in the human trabecular meshwork [44]. One main difference was that in the trabecular meshwork the transverse bands were single instead of double bands. In typical collagen VI assemblies, the transverse bands arise from the electron dense material of the globular N- and C-terminal domains of the collagen type VI molecules and are split into pairs (Figure 4). These double bands are characteristic and indicative of collagen type VI assemblies and come about as a consequence of the axial alignment of the N- and C-globular domains of the outer rod-like regions of collagen type VI tetramers, which are about 30 nm apart axially (Figure 1C,D).

In the aggregates studied here, as well as in those of collagen VI described previously in other tissues [3,5-13], electron dense filaments were seen running perpendicular, or nearly perpendicular, to the transverse bands and crossing them. In the case of the collagen VI assemblies, these filaments were interpreted as arising from the inner and outer rod-like segments of the type VI collagen tetramers that form the assemblies (Figure 5) [37,38].

The many structural similarities between the assemblies in this study of trabecular meshwork and the collagen VI assemblies examined elsewhere [12,37,38,45] suggested that they were all made of collagen VI, with the tetramers

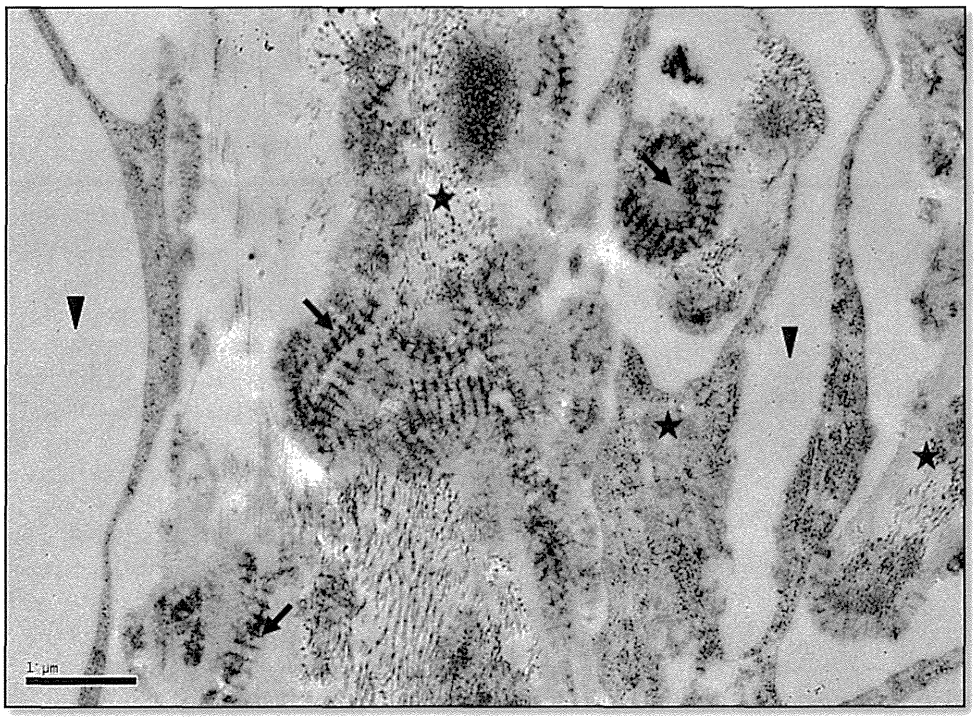


Figure 3. Transmission electron micrograph of the human trabecular meshwork showing a series of parallel layers of connective tissue, known as the trabecular sheets (stars), and intertrabecular spaces forming irregular channels (arrowheads). The trabecular sheets consist of collagen fibrils orientated both transversely and longitudinally and thin trabecular endothelial cells. Type VI aggregates (arrows) are distributed throughout the entire width of the sheet surrounded by collagen fibrils. The black dots dispersed throughout the trabecular meshwork represent 10-nm colloidal gold particles used for tomography. Scale bar = 1 µm.

arranged in essentially the same way. An exhaustive search at the microscope, which included tilting the specimens at different angles, produced clear evidence of single bands splitting into double bands in a small number of assemblies (Figure 4). These double bands were revealed only for a limited tilt angle range, appearing as single transverse bands at a 0° tilt angle, splitting into double bands at higher angles (about 20° in the cases shown in Figure 4), and reverting to single but much narrower bands at higher tilt angles. The axial distance between double bands in these assemblies was not regular, ranging between 112 nm and 85 nm. This would be expected if the tetramers in the assemblies were forming transient links and had not yet settled into a stable configuration. The ratio between the smaller and the larger gaps between the double bands in the most regular assemblies was about 0.2, which is consistent with that of other collagen VI assemblies. The existence of the double bands confirmed the presence of collagen VI in the assemblies.

To achieve a better understanding of the way in which collagen type VI molecules interact with each other in the trabecular meshwork, we generated three-dimensional tomographic reconstructions of the assemblies from single-axis tilt series of electron micrographs. This type of analysis can reveal details of the molecular organization of collagen type VI aggregates that are not accessible from conventional two-dimensional transmission electron microscopy (Figure 5) and can offer new insights into the way collagen type VI molecules are assembled in the matrix of the human trabecular meshwork. In Figure 6 we present one typical three-dimensional reconstruction that we produced of a type VI collagen assembly. Figure 6A shows an 8.57-nm thick slice through the reconstruction, while Figure 6B shows a surface rendering of the same reconstruction. Figure 6C represents a manual segmentation of the same view (see also Appendix 1, Appendix 2, and Appendix 3). In the surface rendering in Figure 6B, the presence of globular domains (highlighted with red arrows) was evident within a transverse band. Globular domains such as these, when not interacting with other material of the extracellular matrix, are likely to be responsible for the double bands seen in typical collagen VI assemblies (and in the assemblies seen in Figure 4). In the trabecular meshwork, the inner rod-like segments of the collagen type VI tetramers assemble with an unsystematic irregular lateral arrangement (Figure 6B; yellow arrowheads), with no evidence of a regular lateral repeat.

Our three-dimensional reconstructions of the trabecular meshwork showed the presence of sulfated proteoglycan filaments, which as well as populating the fibrillar matrix were also seen to co-associate with collagen type VI assemblies (Figure 5, Figure 6, and Appendix 4). The stained filaments were identical in nature to those seen in two-dimensional electron micrographs of trabecular meshwork published

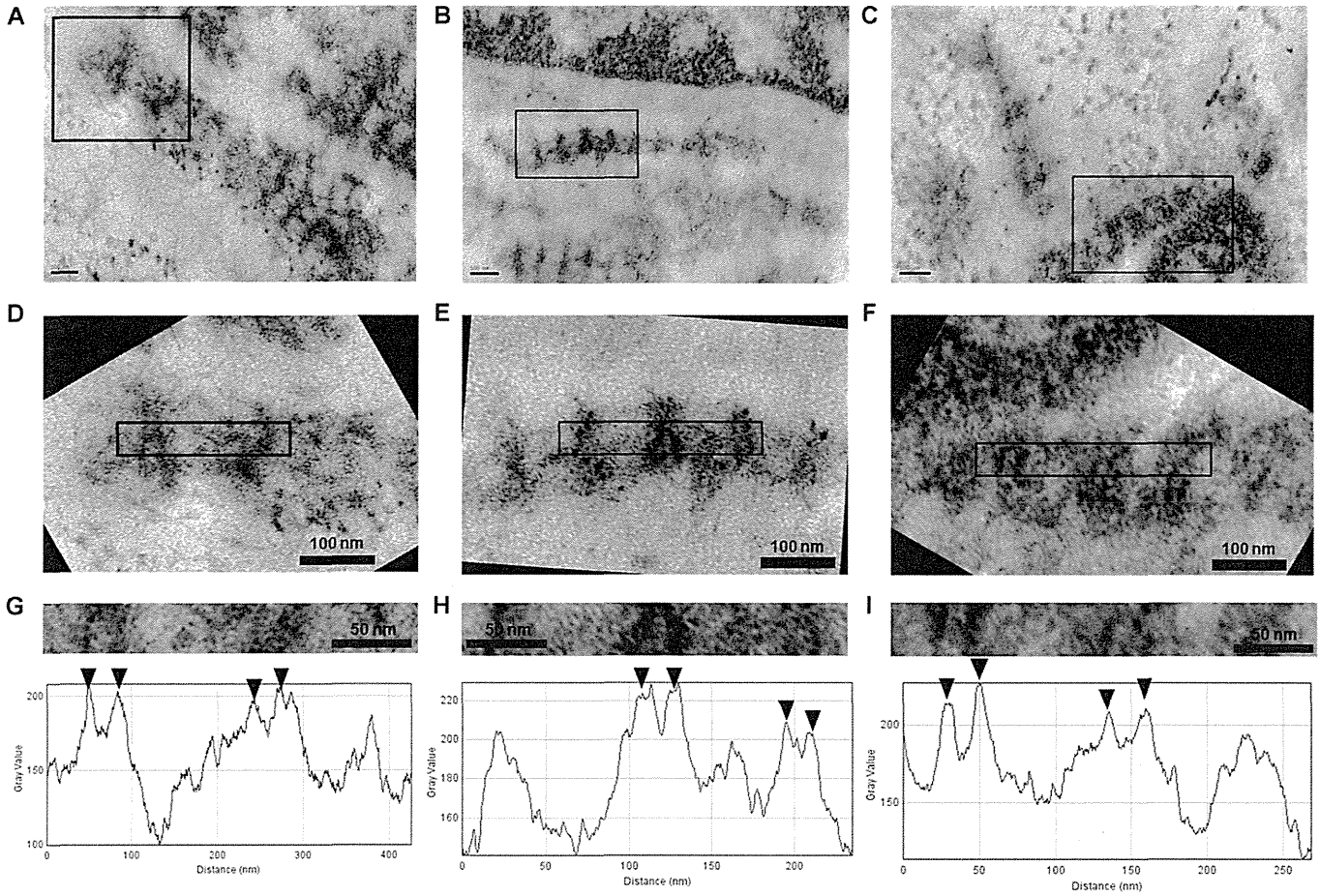


Figure 4. Representative collagen VI assemblies showing pairs of transverse double bands. **A**, **B,** and **C:** Representative collagen VI assemblies found in the human trabecular meshwork during this study (scale bars = 100 nm). The boxed regions in **A**, **B,** and **C** are magnified in **D**, **E,** and **F** (scale bars = 100 nm). **G**, **H,** and **I**: A magnified view and profile density plot of the boxed regions in **D**, **E,** and **F** (scale bars = 50 nm). The horizontal axis of the plots corresponds to distance along the long axis of the rectangular selections. The density profile was obtained by integrating the electron density in the rectangular selection along a vertical path. Arrows indicate peaks on the profile plots that correspond to the dark double transverse band of collagen VI assemblies.

by other investigators [46,47], who confirmed they were proteoglycans by specific enzyme digestion protocols. Proteoglycans were found to associate close to the N- and C- globular domains of type VI collagen as well as to the rod-like segments (Figure 6; see Appendix 4, Appendix 5, and Appendix 6). Moreover, proteoglycans seemed to vary in morphology and size, which is consistent with the fact that different types of proteoglycans can interact with collagen type VI aggregates [47-49]. There was also some evidence of interaction between separate assemblies leading to the formation of larger collagen VI complexes (e.g., Figure 6). In general, it can be seen that the alignment between distinct assemblies within a larger complex occurred by keeping the transverse bands in the axial register (Figure 5 and Figure 6; see Appendix 4, Appendix 5, and Appendix 6).

## DISCUSSION

Type VI collagen can form morphologically distinct aggregates with molecular organization that appears to be related to tissue morphology and physiology [22-28]. Various human pathologies have been associated with collagen type VI [34,35], for example, Bethlem myopathy, an autosomal-dominant, inherited, muscular disorder [50]. There are also indications that type VI collagen assemblies are associated with eye disorders, such as age-related macular degeneration, the leading cause of blindness in the Western world, and Sorsby's fundus dystrophy [37,38]. Previous workers have demonstrated that collagen type VI is a key extracellular matrix component of the trabecular meshwork [51-53]. The current investigation is the first to study the architecture and association with proteoglycans of collagen type VI assemblies

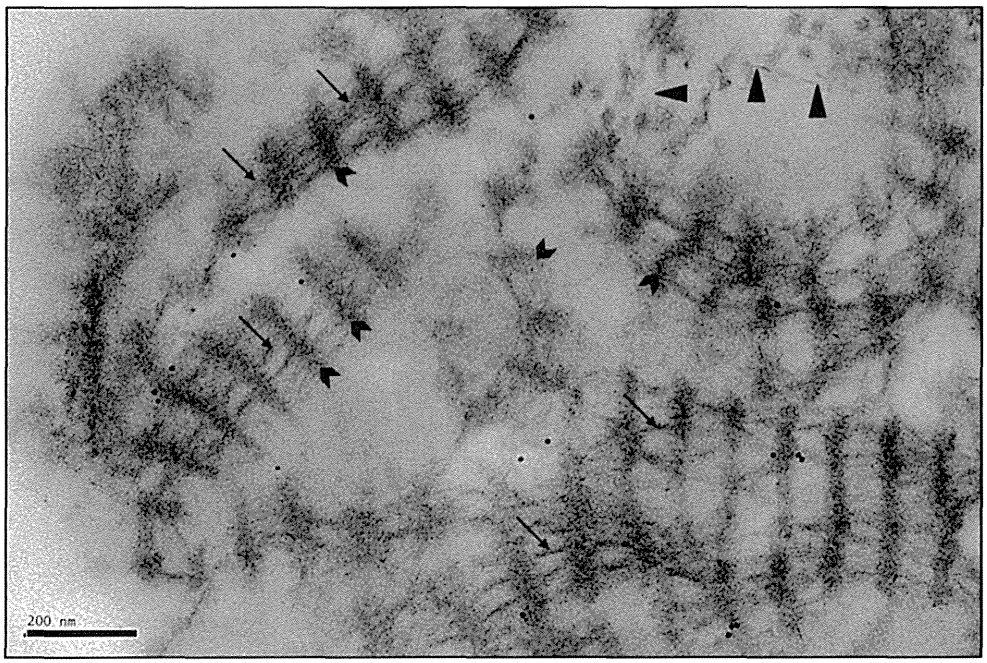


Figure 5. High-magnification longitudinal view of the type VI collagen aggregates in the trabecular sheets. Only single transverse bands are evident (chevrons), and their axial periodicity is approximately 109 nm. The rod-like segments of the collagen VI tetramers (arrows) cross the transverse bands at different angles. Proteoglycans are also seen in the matrix (arrowheads). Several 10-nm gold particles used for tomographic reconstruction appear as black dots in the electron micrograph. Scale bar = 200 nm.

in the human trabecular meshwork by three-dimensional electron tomography.

Our three-dimensional reconstructions showed that collagen type VI tetramers-identified as such from their morphology, periodicity, and the characteristic double-banded structure arising from the arrangement of the globular domains-were aggregated in a more disordered way in the trabecular meshwork compared to other collagen type VI-rich tissues in which the collagen VI assemblies show an extended structural regularity [37,38,45]. This suggests that the molecular or physiologic environment of the trabecular meshwork matrix could interfere with the typical organization of collagen VI assemblies. Our proposed structural model for the collagen VI assemblies in the trabecular meshwork (Figure 7) was based on the interaction of collagen type

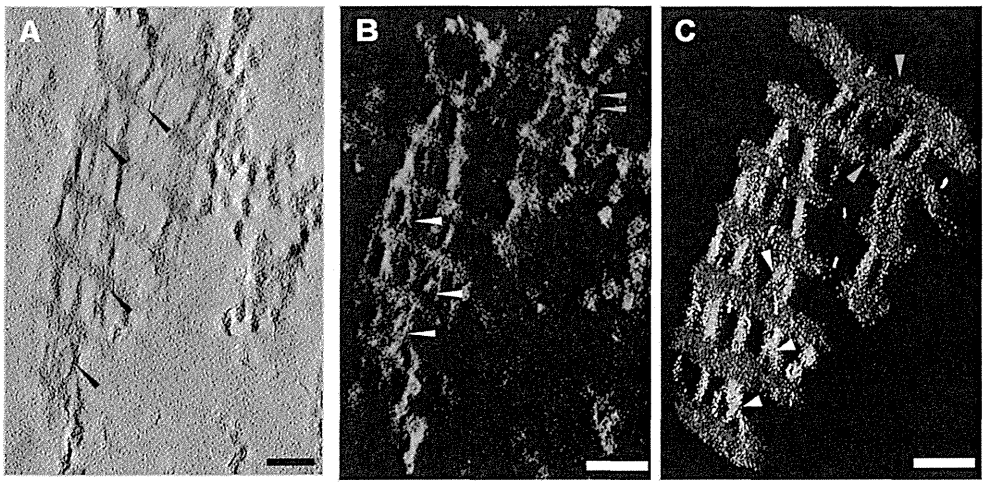


Figure 6. Tomographic reconstructions and segmentation of type VI collagen in the human trabecular meshwork. **A**: An 8.57-nm thick slice through a tomographic reconstruction of a collagen VI assembly. Arrowheads indicate proteoglycans interacting with collagen VI. **B**: Two-dimensional surface representation of a three-dimensional (3D) reconstruction. See Appendix 2 for a 360° view of the reconstruction. The 3D reconstruction has been contrast inverted, and therefore the proteins are shown in white whereas the background is shown in black. The red arrowheads highlight two globular domains. The tetramer's rod-like segments (yellow arrowheads) run across the transverse bands and adopt an irregular organization. **C**: Manually segmented volume of the collagen VI assembly. See Appendix 5 for a 360° view. The transverse bands are shown in blue, the rod-like segments of the collagen VI tetramers in pink, and proteoglycans in yellow. Proteoglycans vary in size and interact with the collagen VI globular domains and the tetramer's rod-like segments. Scale bar = 100 nm.

VI tetramers through their globular domains. These interactions provide stability to the network of type VI collagen. Collagen VI tetramers are the building blocks in this model and they assemble together via noncovalent bonds between the N-terminal globular domains of one tetramer and the C-terminal globular domains of an adjacent tetramer. The electron dense mass of the globular domains would produce, in a different environment, two transverse bands at the position of the C- and N- terminal domains. The fact that single-banded assemblies were largely prevalent suggests that extra material accumulates in the space between the globular domains. It is possible that one or more of the proteins present in the trabecular meshwork interact with the N- and C-terminal globular domains or with the outer rod-like segments of the tetramers, explaining why double-banded aggregates are not always visible in the human trabecular meshwork. It is apparent from our data that there was no extended lateral regularity in the arrangement of the collagen type VI tetramers since not only was their separation variable but so were the relative angles that the inner and outer rod-like segments of the tetramers make with the transverse bands of the assemblies. This might be an effect of the ionic micro-environment of the trabecular matrix itself. In fact, trabecular meshwork cells have the potential to manipulate the aqueous humor outflow by altering the extracellular ionic micro-environment of their matrix, modulating extracellular matrix composition [54], including, for example, the size and degree of extension of meshwork proteoglycans. Following the principle of ionic modulation of flow resistance by the trabecular meshwork cells, a simple supposition would be that changes in the physicochemical properties of the trabecular meshwork would also affect the interactions between the globular domains of the type VI collagen molecules. On this basis, interactions between the globular domains that hold together adjacent tetramers would be disturbed, and this would have an effect on the structural stability of collagen type VI aggregates.

A second possibility is that the structural irregularity of the collagen type VI assemblies in the human trabecular meshwork is the consequence of interactions between the N- and C-terminal domains, which are somehow modulated by other factors or molecules. We should also consider that trabecular meshwork cells sense changes in mechanical stress or intraocular pressure that might trigger remodeling of the matrix to adjust the outflow resistance and maintain intraocular pressure homeostasis. Several matrix proteins are often involved in reorganization of the extracellular matrix and changes in cell-matrix interactions, and some of

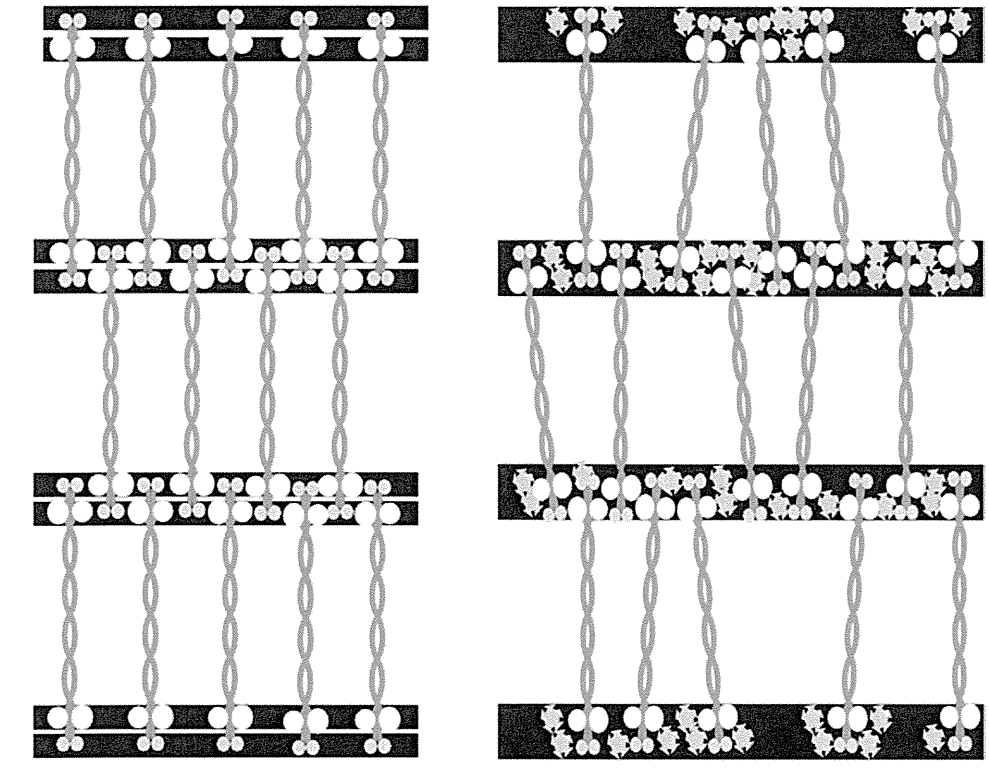


Figure 7. Schematic model of the collagen VI assembly found in human trabecular sheets. N and C termini are depicted in blue and yellow, respectively, and the collagenous triple helices in red. **A**: Model for the double-banded aggregates arising from the alignment of the N- and C-globular domains of the collagen VI tetramers. The black rectangles highlight the position of the transverse bands as seen in the electron micrographs. **B**: Model for the assemblies presenting a single transverse band. The single band arises from a double band with extra material (in green) filling the spaces between globular domains.

these proteins may interact with the collagen VI assemblies. Sulfated proteoglycans have been documented previously in the human trabecular meshwork where they interact with fibrillar collagen [55] and are likely to contribute to aqueous outflow resistance. Here, we demonstrated that these negatively charged macromolecules co-associate with collagen type VI assemblies. In a three-dimensional view, it is clear that while the binding site for a proportion of proteoglycans was located on rod-like segments of the collagen VI tetramers, there were also some proteoglycans associated with the transverse bands where the globular domains of collagen type VI are found. Our findings align with other studies that have shown that collagen type VI interacts with membrane-associated chondroitin sulfate proteoglycan [48], and also with biglycan and decorin [47,49], members of the small leucine-rich repeat proteoglycan family. The interaction of NG2 and collagen type VI is thought to be important in extracellular matrix organization as well as in cell-matrix interactions that determine cell morphology with respect to the matrix. The possibility of multiple proteoglycan binding sites is also in line with previous investigations, indicating that biglycan and decorin are localized near the N-terminal region of the triple helical domain [56] and the following globular domain of type VI collagen tetramers. Previous studies of human trabecular meshwork have indicated a decrease in the numbers of stained cuprolinic blue-proteoglycan complexes with age [47] but an increase in the amount of collagen type VI [57]. These age-related alterations in matrix composition might influence the molecular ultrastructure and interactions in the human trabecular meshwork. It is hoped that new insights into the structure of collagen type VI and associated matrix structures of the trabecular meshwork in the three-dimensional view will shed more light on the function of the tissue and its role in the outflow pathway. As was previously mentioned, the human trabecular meshwork provides flow resistance to aqueous humor leaving the anterior chamber of the eye and thus likely plays a role in the regulation of intraocular pressure [39]. If collagen type VI plays a role in the maintenance of the aqueous humor outflow pathway in the trabecular meshwork, one might hypothesize that alterations in its ultrastructure and interactions with other extracellular matrix components might impact upon pathological changes in the trabecular meshwork.

## APPENDIX 1. 3D SURFACE-RENDERED RECONSTRUCTION OF TYPE VI COLLAGEN AGGREGATES IN THE HUMAN TRABECULAR MESHWORK.

To access the data, click or select the words "Appendix 1." The image has been contrast inverted and therefore the proteins are shown in white whereas the background is shown in black.

## APPENDIX 2. A SURFACE REPRESENTATION OF A 3D RECONSTRUCTION OF THE TILTED TYPE VI COLLAGEN AGGREGATES.

To access the data, click or select the words "Appendix 2." A tilt series was acquired by tilting the specimen around a single tilt axis, in two degree increments over a limited tilt range (+60°, - 60°). See Appendix 3 to view the entire tilt series. The image stack has been contrast-inverted and therefore the proteins are shown in white whereas the background is shown in black. The red arrowheads highlight the double dark transverse bands, formed by N- and C- globular domains of type VI collagen. This feature of collagen VI is not clearly seen in two-dimensional projections. The collagenous triple-helices (yellow arrowheads) run nearly perpendicular to the dark bands.

## APPENDIX 3. 3D SURFACE RECONSTRUCTION OF MULTIPLE TYPE VI COLLAGEN AGGREGATES IN THE HUMAN TRABECULAR MESHWORK.

To access the data, click or select the words "Appendix 3." The image has been contrast-inverted and therefore the proteins are shown in white whereas the background is shown in black.

## APPENDIX 4. TOMOGRAPHIC RECONSTRUCTION AND SEGMENTATION OF TYPE VI COLLAGEN MOLECULES IN THE HUMAN TRABECULAR MESHWORK.

To access the data, click or select the words "Appendix 4." Appendix 6 to view the entire tilt series and the segmented reconstructed volume. (A) Still image from a single slice through a tomographic reconstruction. (B) Manually-segmented reconstructed volume of the collagen VI molecules and proteoglycans, depicted in (A). The dark transverse bands (N- and C- globular domains) are shown in blue, the collagenous triple-helices in pink, and proteoglycans in yellow. Proteoglycans vary in size and interact with the terminal globular domains and/or the triple helices (purple

arrowheads). White arrowheads point to interacting collagenous domains. Lateral associations of adjacent aggregates are indicated by the green arrowheads. A red arrowhead indicates a double band, characteristic of collagen VI. Scale bar=100 nm.

## APPENDIX 5. MANUALLY-SEGMENTED RECONSTRUCTED VOLUME OF THE COLLAGEN VI MOLECULES AND PROTEOGLYCANS IN THE AGGREGATES.

To access the data, click or select the words "Appendix 5." The globular domains are shown in blue, the collagenous triple-helices in pink and the proteoglycans in yellow. This reconstruction was generated by acquiring a tilt series at one degree increments over a tilt range in both directions (+60°, - 60°).

## APPENDIX 6. MANUALLY-SEGMENTED RECONSTRUCTED VOLUME OF THE AGGREGATES IN APPENDIX 3.

To access the data, click or select the words "Appendix 6." The globular domains are shown in blue, the collagenous triple-helices in pink and the proteoglycans in yellow.

## ACKNOWLEDGMENTS

This work was supported by a Cardiff University Professor Sir Martin Evans' President's Studentship to EK, and by collaborative research grants from the Japan Society for the Promotion of Sciences and the Japan Eye Bank.

## REFERENCES

1. Kielty CM, Hopkinson I, Grant ME. Connective tissue and its heritable disorders: Molecular, Genetic and Medical aspects, 2nd ed. Royce, P.M., Steinmann, B.(Eds.), NJ, USA, 2003. pp. 190–2
2. Trüeb B, Schreier T, Bruckner P, Winterhalter KH. Type VI collagen represents a major fraction of connective tissue collagens. Eur J Biochem 1987; 166:699-03. [PMID: 3111851].
3. Keene DR, Engvall E, Glanville RW. Ultrastructure of type VI collagen in human skin and cartilage suggest an anchoring function for this filamentous network. J Cell Biol 1988; 107:1995-06. [PMID: 3182942].
4. Chung E, Rhodes K, Miller EJ. Isolation of three collagenous components of probable basement membrane origin from several tissues. Biochem Biophys Res Commun 1976; 71:1167-74. [PMID: 971306].
5. Odermatt E, Risteli J, van Delden V. Timpl. Structural diversity and domain composition of a unique collagenous fragment (intima collagen) obtained from human placenta. Biochem J 1983; 211:295-02. [PMID: 6870834].
6. Furthmayr H, Wiedemann H, Timpl R, Odermatt E, Engel J. Electron- microscopical approach to a structural model of intima collagen. Biochem J 1983; 211:303-11. [PMID: 6307276].
7. von der Mark H, Aumailley M, Wick G, Fleischmajer R, Timpl R. Immunochemistry, genuine size and tissue localization of collagen VI. Eur J Biochem 1984; 142:493-02. [PMID: 6432530].
8. Hessle H, Engvall E, Type VI. Collagen. Studies on its localization, structure, and biosynthetic form with monoclonal antibodies. J Biol Chem 1984; 259:3955-61. [PMID: 6368554].
9. Engel J, Furthmayr H, Odermatt E, von der Mark H, Aumailley M, Fleischmajer R, Timpl R. Structure and macromolecular organization of type VI collagen. Ann N Y Acad Sci 1985; 460:25-37. [PMID: 3938630].
10. Kuo HJ, Keene DR, Glanville RW. The macromolecular structure of type-VI collagen. Formation and stability of filaments. Eur J Biochem 1995; 232:364-72. [PMID: 7556183].
11. Knupp C, Squire JM. A new twist in the collagen story- the type VI segmented supercoil. EMBO J 2001; 20:372-6. [PMID: 11157744].
12. Knupp C, Pinali C, Munro PM, Gruber HE, Sherratt MJ, Baldock C, Squire JM. Structural correlation between collagen VI microfibrils and collagen VI banded aggregates. J Struct Biol 2006; 154:312-26. [PMID: 16713302].
13. Meek KM, Fullwood NJ. Corneal and scleral collagens—a microscopist's perspective. Micron 2001; 32:261-72. [PMID: 11006506].
14. Jander R, Rauterberg J, Glanville RW. Further characterization of the three polypeptide chains of bovine and human short-chain collagen (intima collagen). Eur J Biochem 1983; 133:39-46. [PMID: 6852033].
15. Chu ML, Conway D, Pan TC, Baldwin C, Mann K, Deutzmann R, Timpl R. Amino acid sequence of the triple-helical domain of human collagen type VI. J Biol Chem 1988; 263:18601-6. [PMID: 3198591].
16. Fitzgerald J, Rich C, Zhou FH, Hansen U. Three novel collagen VI chains, alpha4(VI), alpha5(VI), and alpha6(VI). J Biol Chem 2008; 283:20170-80. [PMID: 18400749].
17. Gara SK, Grumati P, Urciuolo A, Bonaldo P, Kobbe B, Koch M, Paulsson M, Wagener R. Three novel collagen VI chains with high homology to the alpha3 chain. J Biol Chem 2008; 283:10658-70. [PMID: 18276594].
18. Bruns RR. Beaded filaments and long-spacing fibrils: relation to type VI collagen. J Ultrastruct Res 1984; 89:136-45. [PMID: 6100555].
19. Ayad S. The extracellular matrix facts book. Academic Press, London, UK, 1994.
20. Wu JJ, Eyre DR, Slayter HS. Type VI collagen of the intervertebral disc. Biochemical and electron-microscopic